Master of Science in Electrical Engineering
Department of Electrical Engineering, Linköping University, 2016

Boost Control with Turbo Speed Sensor and Electric Wastegate

Bohan Liang and Robin Holmbom

Master of Science in Electrical Engineering

Boost Control
with Turbo Speed Sensor and Electric Wastegate

Bohan Liang and Robin Holmbom

LiTH-ISY-EX--16/4597--SE

Supervisor: **Kristoffer Ekberg**
ISY, Linköpings universitet
Patrik Martinsson
Volvo Car Corporation
Samuel Alfredsson
Volvo Car Corporation

Examiner: **Professor Lars Eriksson**
ISY, Linköpings universitet

Vehicular Systems
Department of Electrical Engineering
Linköping University
SE-581 83 Linköping, Sweden

Intentionally left empty!

Abstract

The purpose of this master thesis is to investigate the possibility to refine the control system of turbochargers in petrol engines by introducing turbo speed measurement. This thesis also investigates possible control enhancement from an electric wastegate actuator compared with a traditional pneumatic actuator. During the thesis work the control problem is divided into 3 sub systems: boost pressure controller, turbo speed controller, and electric actuator controller. The design procedure of the controllers follows model-based method in which a simulation model for engine and a simulation model for electric actuator are used. The designed controller is then implemented and evaluated in an engine test cell. The result of the thesis work shows that the electric wastegate actuator is preferred as it delivers consistent actuation speed and accurate positioning which favours model-based design that requires exact wastegate position. Although the purposed controller structure that uses turbo speed measurement cannot yet achieve faster generation of boost pressure by the end of the thesis work, the use of turbo speed sensor as controller feedback still shows potential to enhance the boost controller and ease the controller design, as the turbo speed measurement can reflect the boost pressure faster and is less sensitive to the disturbances in the air flow.

Acknowledgments

Our examiner Professor Lars Eriksson together with Volvo Car Corporation brought this topic to life and we were lucky to have the honour to carry out the thesis work.

Standing on the finishing line of this challenging and exciting thesis work, we would like to express our deepest gratitude for the generous support we received from our supervisors: Kristoffer Ekberg at Linköping University, Patrik Martinsson and Samuel Alfredsson at Volvo Car Corporation. Their guidance has always been a strong push towards the right direction when we needed it most.

We would also like to show special gratefulness to Tobias Lindell at the division of Vehicular Systems. Many of our achievements have been made possible thanks to his valuable assistance in the engine test cell.

Linköping, June 2016
Bohan Liang and Robin Holmbom

Contents

Notation

Abbreviations

Abbreviation	Description
BSR	Blade Speed Ratio
CUSUM	Cumulative SUM
DFT	Discrete Fourier Transform
IMC	Internal Model Control
MVEM	Mean Value Engine Model
PID	Proportional-Integral-Derivative control
PWM	Pulse-width modulation
RPM	Revolutions Per Minute
RPS	Revolutions Per Second
SI	Spark Ignited
TFP	Turbine Flow Parameter
TSP	Turbine Speed Parameter
VCC	Volvo Car Corporation

1

Introduction

The fundamental part of the thesis is introduced here. The purpose and goal of the thesis, together with the problems that need to be addressed are presented. This chapter also includes related research done by other researchers and institutes within the field of this thesis work. By the end of the chapter the outline of the thesis is presented.

1.1 Purpose and Goal

The purpose of this master thesis is to investigate the possibility to enhance the control system of turbochargers in petrol engines by introducing a tachometer measuring turbo speed, initially for a single turbo system. This thesis also investigates control enhancement for an electrical wastegate actuator compared to a traditional pneumatic actuator.

A major problem today in controlling the wastegate pneumatically is caused by disturbances on wastegate positions. This is due to the fact that pneumatic actuator can't hold the exhaust gas pressure for some operational points. As the wastegate is controlled without position feedback measurements, the control system has little to no knowledge of how well the wastegate actuator is managing its position. Another problem is also unwanted leakage through the wastegate which also can be derived from position uncertainties. This thesis work investigates if an electrical wastegate actuator is able to tackle these problems.

Figure 1.1 presents the fundamental principle outline of how the air and gases circulate the engine with a turbo system.

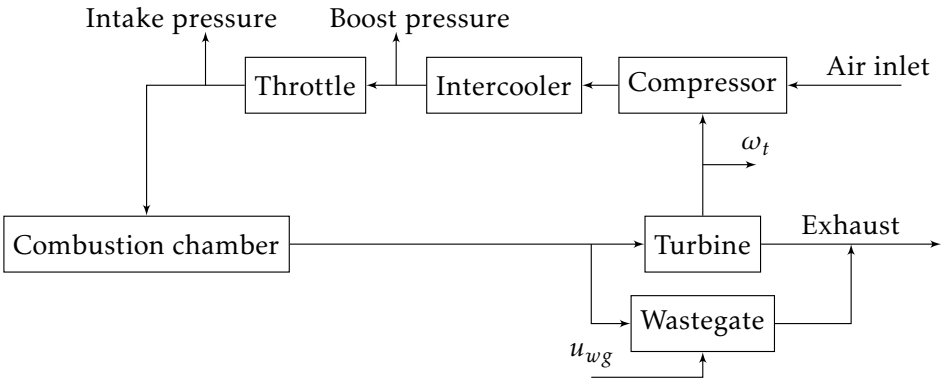

Figure 1.1: *Diagram of the single turbo system, in which one can find the rotation speed measurement ω_t and wastegate actuator u_{wg}. The pressure drop from boost pressure to intake pressure is vital for responsiveness of the boost control.*

The boost pressure affects the driver's experience. A fast response in boost pressure is advantageous. As the boost pressure is generated by the rotation of the turbo, the dynamic of the turbo speed is hypothetically faster than the dynamic of the boost pressure. With the implementation of a turbo speed sensor, given the sensor is sufficiently fast, it may give a faster feedback response to the controller and hence that it is thought to give a faster response and a more robust control. The utilisation of a turbo speed sensor will be implemented in a single turbocharger configuration. The single turbocharger configuration will be evaluated in both simulation environment and in an engine test cell.

An investigation of the feasibility of the above stated possibilities is the main goal of investigation during the thesis work.

1.2 Problem Formulation

Along with the increasing demands for higher vehicle performance and reduced emissions, the development of turbo control systems has gradually gained its importance in the area. One of the unique features in the Volvo Engine Architecture is that all engines, while sharing the same engine block, are able to be tuned into several performance levels using different turbo units. It is therefore of great value that the desired pressures of charged air can be generated with good precision and as fast as possible.

The thesis emphasises on the performance advantages and disadvantages by introducing turbo speed measurement and electric wastegate. To be able to present improvements, one need to perform measurements of today's performance. This measurement is called baseline measurement. Comparisons that is based on baseline measurements can be used to present differences and improvements. The questions that needs to be answered in the thesis work are:

- How to establish a fair measurement baseline for further benchmark comparison?
- What are the control strategies that utilise turbo speed measurement?
- How is the performance achieved with turbo speed measurement, electric wastegate actuator, and both combined?
- How does the performance differ from the baseline controller?

1.3 Related Research

Related research that previously treated similar problems is used as a basis for the work in this thesis. Different engine models for a mean value engine model is well described in the book Eriksson and Nielsen (2014). As a base for the control strategies the books Enqvist et al. (2014) and Glad and Ljung (2014) are being used where different control strategies are presented.

1.3.1 Turbo Speed Measurement

Many studies mentioned that it is common to measure the turbocharger speed for the purpose of component modelling and few have proposed the use of direct speed measurement in turbo control. According to Cavina et al. (2008) this is due to the increasing cost of the system component. The non-intrusive turbo speed measurement presented in the same article made use of correlation between rotational speed and acoustic emission. The purpose of the speed measurement was however not the control of the turbo unit but for preventing the turbocharger from going over the allowed speed limit. In this thesis the speed measurement is directly used for boost control.

Ponti et al. (2014) pointed out that most non-intrusive method for speed measurements only achieves the mean value of the speeds and the actual speed fluctuations from unsteady flows remains unknown. The knowledge of speed fluctuations can overcome errors in low-flow range instabilities and uncertainties in interpolation and extrapolation of maps as reported in Dehner et al. (2013) and Moro et al. (2009) respectively. Ponti et al. (2014) also claimed that the knowledge of speed fluctuations can aid calculation of the actual power delivered by the turbine. In this thesis as the turbo speed is measured directly, the advantages described above can be automatically gained.

1.3.2 Electric Wastegate Actuator

As stated by Ni et al. (2013) the use of electric wastegate actuator addresses the disadvantages posed by traditional vacuum-actuated wastegate such as position pulsations and leakage. The article also concludes that the electric actuator normally actuates much faster than the vacuum actuator. The speed of the wastegate movements can also be controlled freely, which for instance can be used to decelerate when approaching position limits of the wastegate thus reduces wear. As

the control of wastegate position become a feedback system, with proper tuning the position fluctuations can also be mitigated.

In Capobianco and Marelli (2007) the modelling of wastegate and turbine mass flow and efficiency during steady and unsteady flows are discussed. The article also includes analysis of wave propagation phenomena in the turbine components.

The turbocharger controller strategy suggested by Karnik and Jankovic (2012) proposed an architecture based on Internal Model Control (IMC) for charged air pressure by controlling the wastegate positions. The key principle that was described in the article is that a first order system can be used as the engine model in the IMC. Firstly a physical model of the engine is produced in order to find important state variables during engine operations. The model is then numerically simplified in a way that the resulted equations can be inverted to act as feedforward information. The results in the article shown promising potential of IMC in the control problem as the IMC eliminated the overshoot in boost pressure by a small amount of response time trade-offs. If a reasonable amount of boost pressure overshoot is otherwise allowed, the reproduction of the algorithm proposed in the article may aid the development in this thesis work.

Many ideas suggested by Ni et al. (2013) have aided the design of wastegate actuator controller in this thesis work. The IMC controller for the turbo speed controller that makes use of electric wastegate actuator is partially inspired by the approaches in Karnik and Jankovic (2012).

1.3.3 Turbocharger Component Modelling and Simulation

To evaluate different strategies during this thesis work a Mean Value Engine Model (MVEM) will be used. According to Eriksson and Nielsen (2014) mean value models have been around since the 1970s, but after Hendricks (1986) the term MVEM was attributed to Elbert Hendricks. One of the first MVEM for a Spark Ignited (SI) engine is described in Hendricks and Sorenson (1991). Modelling of turbochargers in MVEM were described by, among others, Jensen et al. (1991) and Müller et al. (1998). The performance of a turbocharger is often only given in data maps by the producer with very few data points. Interpolation and extrapolation is needed to get a good representation of the turbocharger. Moraal and Kolmanovsky (1999) presents an overview of curve fitting methods that were available at that time. The paper also mentioned how important the compressor flow rate modelling is since it is a crucial part of the overall engine model. Many different compressor models were described in Leufven (2013). To get better interpolation and extrapolation of the data maps a physics approach is often needed. In the paper Hadef et al. (2012) they describe new methods of interpolation and extrapolation by integrating more physics. Meddahi et al. (2015) is mostly based on Hadef et al. (2012) but it also takes into account for thermodynamic and aerodynamic losses for the compressor models.

To model the behaviour from wastegate position to the pressure after the compressor the book Eriksson and Nielsen (2014) is used to derive relationships. In Thomasson et al. (2009) a description of how to model a transfer function from

wastegate actuator to boost pressure is given. This model is then used in an IMC that turns out to be a Proportional-Integral-Derivative controller (PID).

A model of the turbo speed as a first order delay to combustion chamber intake air has been done in Togai and Fujinaga (2015) were it was shown that it produced good fit for low engine speeds but not as good for higher engine speeds. A model of the relationship between turbo speed and the pressure ratio over the compressor is also shown in Togai and Fujinaga (2015).

The development phase in this thesis consists mostly of simulation environment and validations with an engine in a test cell. In Andersson (2005) a method to validate the simulation environments with map- and dynamic data is described.

Many improvements have been done on the engine simulation environment used during the thesis work. The above stated literatures have provided valuable suggestions and methodologies within modelling and model validation.

1.4 Thesis Outline

The thesis consists of 6 chapters and their contents described below.

- **Chapter 1 - Introduction**
  Presents the problem formulation and literature studies.
- **Chapter 2 - Background**
  The chapter provides background information of the thesis work and system overview of the experimentation.
- **Chapter 3 - Model Theory**
  Theories for the models evaluated in this thesis are presented in this chapter.
- **Chapter 4 - Control Theory**
  Theories for the control strategy suggestions that await evaluations in this thesis are presented in this chapter.
- **Chapter 5 - Results**
  Results of the different control strategies applied in both simulation and real life engine are evaluated and presented in this chapter. Validations and preferences of models from *Chapter 3 - Model Theory* are also discussed in this chapter. Comparison between simulations and engine tests is also presented.
- **Chapter 6 - Conclusions and Future Work**
  This chapter presents the conclusions that are made from the results based on the problem formulation presented in the introduction chapter.

2

Background

In this chapter the basic concepts for turbocharging and its components are described. As the thesis work uses model-based approaches, the MVEM model used for simulation is also introduced.

2.1 Turbo

The main part in this thesis involves turbochargers in a spark ignited (SI) engine. Development today has an increasing focus on emission reduction and fuel efficiency. Smaller engines are more efficient than bigger ones but the problem is their insufficient ability to supply the air mass for the combustion as a bigger engine. A trend in the industry is therefore to increase efficiency by downsizing engines and equipping them with turbochargers to achieve same performance as bigger engines. The turbocharger increases the air density in the intake, so that the intake system can bring enough air mass to ignite the needed fuel for optimal combustion. A turbocharger consists of a turbine and a compressor connected to each other through a shaft. The turbine extract energy from the exhaust gases and delivers the energy to the compressor through the shaft between them. A turbocharged engine has a drop in torque for low engine speeds, which is due to a region of instability in the compressor called surge. For a single turbocharger configuration this results in a design trade-off between low speed torque and maximum engine power. For more information about turbochargers see e.g. Eriksson and Nielsen (2014), Leufven (2013) or Andersson (2005).

2.1.1 Compressor

The compressor is the part of the turbocharger powered by the rotating turbine shaft and compresses air into the intake manifold. Whilst the air that is being

compressed and released after the compressor blades will have higher pressure than before, the temperature of the air is also increased. It is therefore common to use an intercooler (also called aftercooler) to exchange heat from the intake air and further increase the air density.

Along the air intake where the compressor is involved, much measurement information is already available from the original sensors on production engines. The measurements that can be used by the control system for the turbocharger are: air mass flow, ambient pressure, temperature before the compressor, boost pressure, and pressure in the intake manifold. Good observability can be gained from these measurement which eases the compressor modelling.

According to Eriksson and Nielsen (2014) the compressor operation is limited by the following four factors:

- **Maximum speed:** rotation speed needs to be limited to prevent mechanical damage.
- **Surge:** the unstable operation under too high pressure ratio which causes the flow to reverse.
- **Choking:** maximum flow is limited by the predominant sonic condition.
- **Restriction:** the compressor acts as flow restriction as the pressure ratio becomes too low.

Compressor surge can be avoided by controlling an extra valve that redirect the air back to before the compressor. This mechanism is called anti-surge or bypass valve and is typically binary, in other words it can be either opened or closed.

2.1.2 Turbine

Similar to compressor, the turbine in a turbocharger is also a flow device that exchanges fluid work with mechanical work. It makes use of energy in the exhaust gas from the combustion chamber to power the rotation of the turbine shaft. As described by Eriksson and Nielsen (2014) the energy is harvested from expanding gases with high pressure and temperature and leaves behind gases with lower pressure and temperature. This is a non-ideal process as not all energy from the exhaust gases can be made use of. The efficiency of the turbine are consistently affected by heat transfers to the surroundings and mechanical losses.

The power of the turbocharger is controlled by the wastegate installed on the exhaust side of the turbocharger. Eriksson and Nielsen (2014) describes the wastegate as a flow regulating device that allows part of the exhaust mass flow to bypass the turbine by varying the wastegate valve, controlling the turbo speed and thereby increase or decrease the boost pressure. The position of the wastegate valve is normally controlled by a vacuum actuator or an electric actuator.

Unlike the compressor, it is generally uncommon to include direct temperature and pressure measurements around the turbine in a production engine due to the extreme thermal conditions for the sensors. This implies that information from the exhaust part of the production engines can only be achieved

through modelling, which demands good performance of the turbine model and the wastegate model.

2.2 Mean Value Engine Model

As mentioned in Section 1.3.3 one of the first MVEM for an SI engine was first mentioned in Hendricks and Sorenson (1991). An MVEM models the average engine characteristics during one or several engine cycles and is often used to model and simulate engines. The MVEM used in this master thesis is originally developed by the staff at the division of Vehicular Systems at Linköping University and in various student projects. The MVEM seen in Figure 2.1 is built along the air mass flow. It is possible to follow the air flow from the air filter at the top right hand corner clockwise to the exhaust pipe at the top left hand corner. As Andersson (2005) mentioned it is worth noticing that the turbocharger shaft dynamics block is shown in the middle where the exhaust side connects with the intake side. Because of this, model errors at the turbine side can propagate back to the intake side. This master thesis surrounds the turbocharger and therefore a well described turbocharger is of importance to get a good simulation representation of the real engine from Volvo Car Corporation (VCC). The MVEM will be used in this master thesis to be able to easily test different control approaches. Also to be able to develop a good methodology that is of help when making tests in the engine test cell.

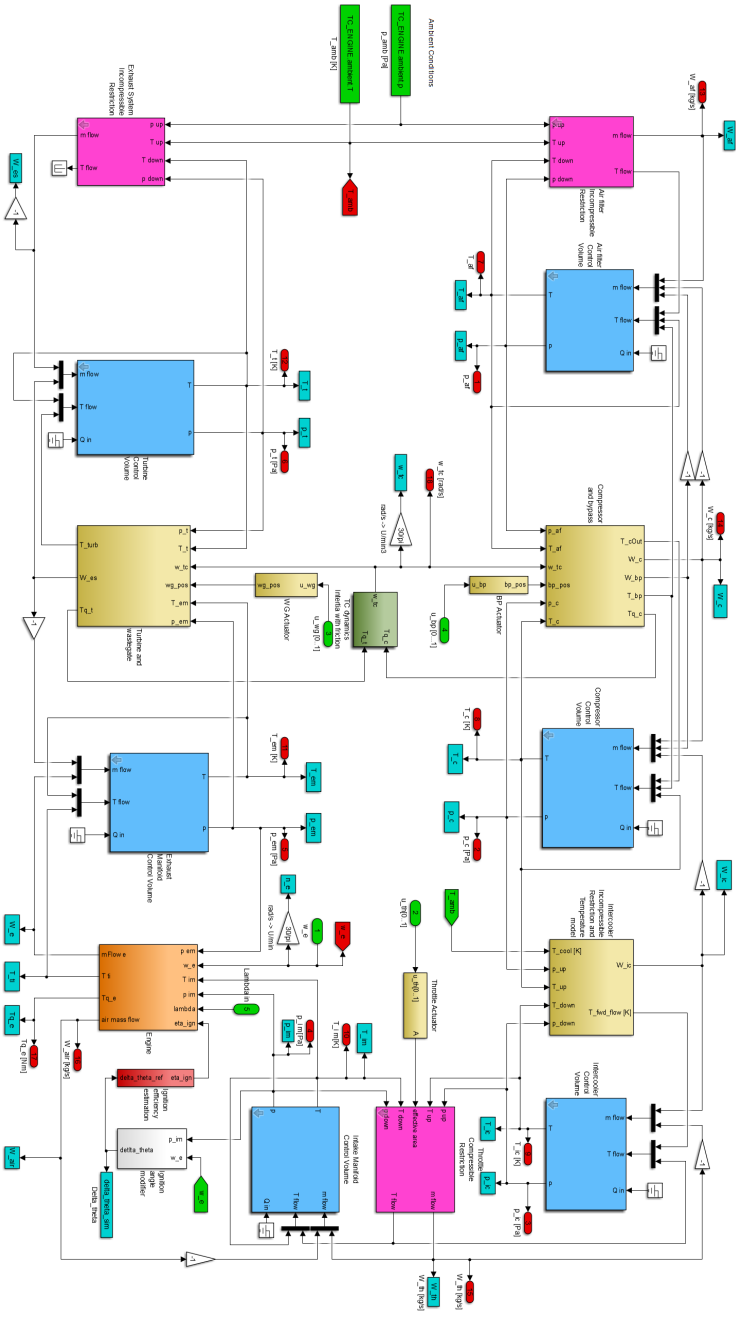

Figure 2.1: *Overview of the Simulink MVEM used in this master thesis. Air filter at the top right corner and exhaust pipe at the top left corner. Turbocharger shaft dynamics block can be seen in the center.*

2.3 Wastegate and Wastegate Actuator

The wastegate is an important design feature of the turbocharger which serves the purpose of regulating the boost pressure. The position of the wastegate valve affects the flow distribution between the turbine and the wastegate itself. Figures 2.2 and 2.3 show the operation of the wastegate from after the turbine. The perspective of the figures can be interpreted as if the exhaust gas from this part of the turbocharger is blowing towards the reader. When the wastegate is closed, as Figure 2.2 illustrates, the entire exhaust gas flow is directed through the turbine, making it spin faster and thus enables the compressor to generate higher boost pressure.

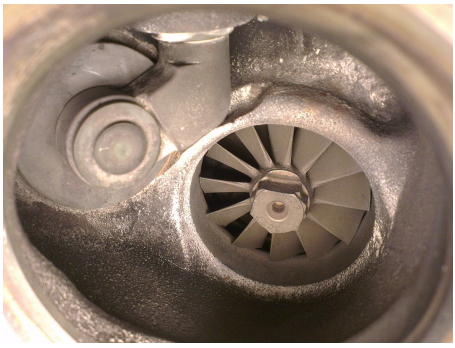

Figure 2.2: *Closed wategate: the valve covers the bypass entirely. Exhaust gas is guided through the turbine in order to increase the boost pressure.*

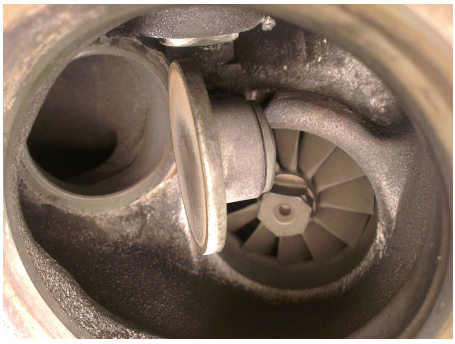

Figure 2.3: *Open wastegate: a fully opened wastegate. More flow is diverted through the bypass rather than propelling the turbine, resulting in a decreased power transfer to the compressor.*

The wastegate can be gradually opened to allow some part of the exhaust gas to bypass the turbine to manage control of the turbo speed. When the gap between the valve and the wastegate opening increases, more flow is diverted through the wastegate, resulting in lower pressure difference after the turbine. Figure 2.3 demonstrates a fully opened wastegate. The positioning of the wastegate valve is actuated by an external actuator, called wastegate actuator. The most common actuator for this application is a Pulse-Width Modulation (PWM), controlled pneumatic actuator. The component is sometimes also called vacuum actuator as it is connected to a high power vacuum pump with a PWM controller which regulates the feeding pressure to the actuator. The vacuum nozzle can be clearly seen in Figure 2.4. The movement of the long rod to the upper-left corner of the picture actuates the wastegate valve.

As mentioned by Thomasson et al. (2013) the exact position of the rod is seldom linear to the PWM duty cycle of the control signal, and the position accuracy may not be exempt from variations of the battery voltage that powers the pump. The movement of the rod is inconsistent when coupled to the wastegate valve. It

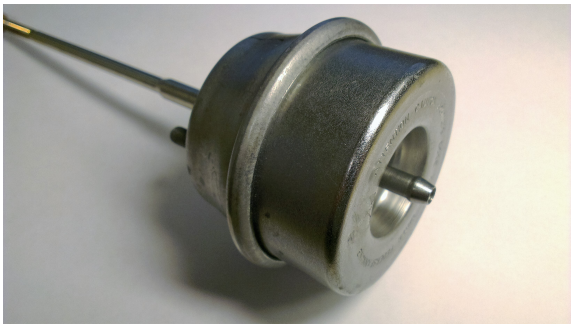

Figure 2.4: *Pneumatic actuator for wastegate valve with control rod to the left and vacuum-feeding nozzle to the right.*

can be observed that the positions follow hysteresis phenomenon, in other words the actuation depends on if the wastegate previously was opened or closed. The position of wastegate in motion will also depend on whether the input signal is increasing or decreasing. To actuate the wastegate electrically with position feedback may remedy the above mentioned drawbacks and will be further studied in this thesis work.

3

Model Theory

In this chapter models for the compressor, the turbine, and the electric wastegate actuator are presented. A relative error is often used to described how well the models agree with the measurements and is defined as

$$e = \frac{|x_{model} - x|}{x} \tag{3.1}$$

where x_{model} is the model output and x is the measured value. If x is a small value close to zero the relative error is not representing the results well. In these cases absolute error is used and is defined as

$$e = |x_{model} - x| \tag{3.2}$$

Data normalisations are performed according to

$$x_{norm} = \frac{x}{x_{max}} \tag{3.3}$$

where x is the value and x_{max} is the maximum value of that quantity.

3.1 Compressor Modelling

Performance of the compressor is often only given in performance maps. The given maps are usually the compressor efficiency against compressor mass flow and pressure ratio against compressor mass flow. The pressure ratio is defined as

$$\Pi_c = \frac{p_{ac}}{p_{bc}} \tag{3.4}$$

where p_{ac} is pressure after the compressor and p_{bc} is pressure before the compressor. As mentioned in Section 2.1.1 the compressor is limited by four different

factors: maximum speed, choking, surge and restriction. These different factors can either be modelled or neglected, depending on for what operating points the model is going to be used for. In the performance maps the mass flow and the speed are usually normalised. In this thesis the normalisation is performed with reference pressure, p_{ref}, and reference temperature, T_{ref}. The normalised quantities are called corrected mass flow and corrected speed. Reference conditions are given in the performance maps to the turbochargers used in this thesis. Relationship between corrected quantities and real quantities are given by

$$\dot{m}_c = \dot{m}_{c,corr} \frac{p_{bc}/p_{ref}}{\sqrt{T_{bc}/T_{ref}}} \qquad N_c = N_{c,corr} \sqrt{T_{bc}/T_{ref}} \tag{3.5}$$

where $\dot{m}_c$ is compressor mass flow, $\dot{m}_{c,corr}$ is corrected compressor mass flow, N_c is compressor speed in revolutions per second (RPS), $N_{c,corr}$ is corrected compressor speed and T_{bc} is the temperature before the compressor.

Dimensionless quantities introduced by Winkler (1977) are often used to model the compressor. These are the dimensionless flow rate, Φ, and dimensionless head parameter, Ψ. They are defined as

$$\Delta h_{0s} = c_p T_{bc} \left(\left(\frac{p_{ac}}{p_{bc}} \right)^{\frac{\gamma-1}{\gamma}} - 1 \right) \tag{3.6}$$

$$\Psi = \frac{\Delta h_{0s}}{N^2 D^2} = \frac{c_p T_{bc} \left(\left(\frac{p_{ac}}{p_{bc}} \right)^{\frac{\gamma-1}{\gamma}} - 1 \right)}{N^2 D^2} \tag{3.7}$$

$$\Phi = \frac{\dot{m}_c}{\rho_{bc} N D^3} = \frac{\dot{m}_c R T_{bc}}{N D^3 p_{bc}} \tag{3.8}$$

in Eriksson and Nielsen (2014). In (3.6)-(3.8), N is the compressor speed in RPS, D is the compressor diameter, γ is the ratio of specific heats, $\gamma = \frac{c_p}{c_v}$, where c_p is the specific heat at constant pressure and c_v is the specific heat at constant volume, ρ_{bc} is the air density before the compressor and R is the ideal gas constant. The specific energy that is consumed by an adiabatic compression process, Δh_{0s}, from a state with pressure, p_{bc} and T_{bc} to another state with pressure, p_{ac}.

3.1.1 Compressor Mass Flow Model

In the given MVEM for this thesis the compressor mass flow model used was the basic ellipse model described in Eriksson and Nielsen (2014). Where the relationship between Ψ and Φ defined in (3.7)-(3.8) are approximated with an ellipse as

$$\left(\frac{\Phi}{k_1} \right)^2 + \left(\frac{\Psi}{k_2} \right)^2 = 1 \tag{3.9}$$

where k_1 and k_2 are tuning parameters. First calculate Ψ with (3.7) and then solve (3.9) for Φ and then solve (3.8) for $\dot{m}_c$ gives

$$\Phi = k_1 \sqrt{1 - \left(\frac{\max(\min(\Psi, k_2), 0)}{k_2} \right)^2} \tag{3.10}$$

$$\dot{m}_c = \frac{N D^3 p_{bc}}{R T_{bc}} \Phi \tag{3.11}$$

The use of max and min in (3.10) are to make sure that it gives a solution in the first quadrant for the ellipse in (3.9).

To improve the MVEM the extended ellipse model described in Eriksson and Nielsen (2014) was implemented. This model uses 14 parameters that needs to be estimated. Leufven (2013) studied this extended ellipse model further in the restriction and choke region. It can be hard to determine these 14 parameters that needs to be calculated in this model because the initial values are of importance to find a reasonable solution. The extended ellipse model is described as

$$c_0 = c_1 + c_2 c_5^{c_3} - c_4 c_5 \tag{3.12}$$

$$\dot{m}_C(N_{corr}) = \begin{cases} c_1 + c_2 N_{corr}^{c_3} & , N_{corr} \leq c_5 \\ c_0 + c_4 N_{corr} & , N_{corr} > c_5 \end{cases} \tag{3.13}$$

$$\Pi_C(N_{corr}) = c_6 + c_7 N_{corr}^{c_8} \tag{3.14}$$

$$\dot{m}_Z(N_{corr}) = c_9 N_{corr}^{c_{10}} \tag{3.15}$$

$$\Pi_Z(N_{corr}) = 1 + \Pi_{c,max} \left(c_{11} N_{corr,norm}^{c_{12}} \right) \tag{3.16}$$

$$C(N_{corr}) = c_{13} + c_{14} N_{corr}^{c_1 5} \tag{3.17}$$

$$\dot{m}_{corr}(N_{corr}) = \dot{m}_Z + (\dot{m}_C - \dot{m}_Z) \max \left(0.01, \left(1 - \left(\frac{\Pi_c - \Pi_C}{\Pi_Z - \Pi_C} \right)^C \right) \right)^{\frac{1}{C}} \tag{3.18}$$

where c_i is the parameters to be determined. Π_Z and Π_C describes the zero slope line and choke line for the pressure ratio, $\dot{m}_Z$ and $\dot{m}_C$ describes the zero slope line and choke line for the mass flow.

3.1.2 Compressor Efficiency Model

The model used for the compressor efficiency in the MVEM is a variant of the quadratic form compressor efficiency model described in Eriksson and Nielsen (2014). The variant used in the MVEM

$$\chi(\dot{m}_{c,corr}, \Pi_c) = \begin{bmatrix} \dot{m}_{c,corr} - \dot{m}_{c,corr,max} \\ \sqrt{\Pi_c - 1} + 1 - \Pi_{c,max} \end{bmatrix} \tag{3.19}$$

$$\eta_c(\chi) = \max \left(\eta_{c,max} - \chi^\intercal Q_\eta \chi, \eta_{c,min} \right) \tag{3.20}$$

where $Q_\eta \in \mathfrak{Re}^{2\times 2}$ is a symmetric and positive definite matrix. $\dot{m}_{c,corr,max}$, $\Pi_{c,max}$, $\eta_{c,max}$, $\eta_{c,min}$ and the elements in Q_η are tuning parameters.

3.2 Turbine and Wastegate Modelling

The manufacturer of the turbocharger usually present the performance of the turbine by providing a set of mapped data. The turbine data map describes turbine flow characteristics and turbine efficiency as functions of turbine pressure ratio defined as

$$\Pi_t = \frac{p_{em}}{p_t} \tag{3.21}$$

where p_{em} is the pressure in the exhaust manifold right before the turbine and p_t is the pressure after the turbine. As the gas normally flows from the engine block towards the exhaust pipe outlet, the relation $\Pi_t \geq 1$ should hold.

The data consists of steady state measurements and was gathered under controlled conditions. For modelling of the turbine the mapped data is valuable as some of the measurement conditions such as extreme pressures and speeds may not be achievable by normal engine operations. The inclusion of these conditions is important for the generalisation of the overall model, as the model includes wider range of operating conditions and thus can be implemented into different type of vehicles such as family cars and sport cars. Should the engine operate outside the normal conditions, the model-based control system that have information of the extreme conditions is also capable of making more accurate judgement and adjustment. The general model can therefore be estimated by processing the mapped data and then be further polished by engine tests.

3.2.1 Turbine and Wastegate Flow Models

The mass flow through the turbine is commonly normalised to the controlled conditions where the measurements were performed under. In Eriksson and Nielsen (2014) the normalised mass flow is called corrected mass flow or Turbine Flow Parameter (TFP). The calculation of TFP is defined as

$$TFP = \frac{\dot{m}_t \sqrt{T_{em}}}{p_{em}} \tag{3.22}$$

where $\dot{m}_t$ is the mass flow through the turbine. T_{em} and p_{em} in (3.22) are temperature and pressure in the exhaust manifold right before the turbine.

Correspondingly the turbine speed is also commonly normalised to the controlled conditions and the normalised turbine speed is called corrected speed or Turbine Speed Parameter (TSP). The calculation of TSP is defined as

$$TSP = \frac{N}{\sqrt{T_{em}}} \tag{3.23}$$

where N is the turbine speed. In continuation of the thesis work the abbreviations TFP and TSP will be used.

Eriksson and Nielsen (2014) thoroughly explained and compared different methodologies for modelling of the turbine from mapped data. The introduced methods can be summarised roughly into two categories: models with physical motive and non-physical curve fittings.

The model with physical motive that was first proposed by this thesis work is based on compressible flow through a restriction. The turbine is considered as restriction in this case. The basic form of compressible restriction flows is as follows

$$TFP = A_{eff,t}(\Pi_t, TSP)\frac{1}{\sqrt{R_{exh}}}\Psi(\Pi_t), \qquad \Psi(\Pi_t) = \Psi_0(\Pi) \tag{3.24}$$

with

$$\Psi_0(\Pi) = \sqrt{\frac{2\gamma}{\gamma-1}\left(\Pi^{\frac{2}{\gamma}} - \Pi^{\frac{\gamma+1}{\gamma}}\right)}, \qquad \Pi = \max\left(\frac{1}{\Pi_t}, \left(\frac{2}{\gamma+1}\right)^{\frac{\gamma}{\gamma-1}}\right)$$

where R_{exh} is the specific gas constant of exhaust gas and γ is the specific heat ratio of the gas. The model treats the effective area, $A_{eff,t}$, as function of pressure ratio and TSP, and is defined as

$$A_{eff,t}(\Pi_t, TSP) = (k_{1,1}TSP + k_{1,2})\Pi_t + k_{2,1}TSP + k_{2,2} \tag{3.25}$$

The free parameters $k_{i,j}$ are then estimated to best fit the data map.

The second model proposal follows the curve-fitting approach. The model adapts to the square root appearance of the mass flow in the data map and neglects the dependency on speed. This speed dependency is according to Eriksson and Nielsen (2014) small and caused by centrifugal forces along the turbine blades that oppose flow direction. The model is defined as follows

$$TFP = k_0\sqrt{1 - \frac{1}{\Pi_t}^{k_1}} \tag{3.26}$$

where k_0 and k_1 can be estimated to fit the data map.

An orifice flow model is proposed by Karnik and Jankovic (2012) to describe the exhaust gas flow through the wastegate. The model structure is also mentioned by Eriksson and Nielsen (2014) as compressible flow and the equations are similar to (3.24) with the exception in effective area which in wastegate modelling is a function of wastegate valve position denoted by

$$A_{eff,wg} = f_{wg}(wg_{pos}) \tag{3.27}$$

To simplify the modelling procedure the position of the wastegate valve wg_{pos} in (3.27) can be normalised, in which 0 corresponds to a fully closed wastegate and 1 is fully opened wastegate. Additionally the following relationship shall apply to account for zero flow through a closed wastegate

$$f_{wg}(0) = 0 \tag{3.28}$$

To estimate and validate the wastegate model it is required to have knowledge of the actual mass flow through the opening. To acquire direct flow measurement in this part of engine is difficult due to the extreme thermal conditions. However the observation of mass flow from the combustion chamber is available and

the wastegate is nothing but a flow diverting device. With an turbine mass flow model available, the mass flow through the wastegate is simply

$$\dot{m}_{wg} = \dot{m}_e - \dot{m}_t \tag{3.29}$$

where $\dot{m}_e$ is total exhaust mass flow from combustion chambers and $\dot{m}_t$ is the modelled turbine flow.

Karnik and Jankovic (2012) suggested the following simple linear model for the wastegate effective area

$$A_{eff,wg} = wg_{pos} A_{eff,max} \tag{3.30}$$

where $A_{eff,max}$ is the maximum achievable opening area of the wastegate valve and can be estimated by using steady state measurement data from an engine test cell.

The linear relation can be further expanded to n-degree polynomial model to increase fitness to measured data as long as (3.28) is satisfied.

3.2.2 Turbine Efficiency Models

The knowledge of the turbine efficiency is vital for estimation of pressure and temperature after the turbine as well as estimation of the power delivery to the compressor. As mentioned in Section 2.1.2 the turbine harvests energy from gases with high pressure and temperature in the exhaust manifold and leaves behind gases with lower pressure and temperature. The process is non-ideal and the efficiency of the turbine is defined in Eriksson and Nielsen (2014) as the ratio between actual power delivered to the compressor and the power delivered by an ideal process. Noteworthy the mechanical losses are already accounted in the efficiency. The ideal process in this case is isentropic expansion and the power delivered by a such ideal process is defined as

$$\dot{W}_{t,ideal} = \dot{m}_t c_{p_{exh}} T_{em} \left(1 - \frac{1}{\Pi_t}^{\frac{\gamma-1}{\gamma}} \right) \tag{3.31}$$

where $c_{p_{exh}}$ denotes the specific heat of exhaust gas. From (3.31) one can also acquire the ideal isentropic specific enthalpy change

$$\Delta h_{is} = c_{p_{exh}} T_{em} \left(1 - \frac{1}{\Pi_t}^{\frac{\gamma-1}{\gamma}} \right) \tag{3.32}$$

Eriksson and Nielsen (2014) proposed a model structure for turbine efficiency which makes use of the turbine's Blade Speed Ratio (BSR). The BSR is derived in the following way

$$BSR = \frac{\omega_t r_t}{\sqrt{2 c_{p_{exh}} T_{em} \left(1 - \frac{1}{\Pi_t}^{\frac{\gamma-1}{\gamma}} \right)}} \tag{3.33}$$

The turbine efficiency with BSR is then

$$\eta_t(BSR) = \eta_{t,max}\left\{1 - \left(\frac{BSR - BSR_{opt}}{BSR_{opt}}\right)^2\right\} \tag{3.34}$$

where $\eta_{t,max}$ and BSR_{opt} can be obtained from the mapped data. $\eta_{t,max}$ is taken as the maximum efficiency registered in the dataset. BSR_{opt} is taken as the maximum BSR calculated from dataset by applying (3.33).

Another model that aims to provide robust interpolation and extrapolation of the manufacturer's data maps is suggested by Hadef et al. (2012). The model is based on the definition that the turbine efficiency is the ratio of the specific enthalpy change over the isentropic enthalpy change

$$\eta_t = \frac{\Delta h}{\Delta h_{is}} \tag{3.35}$$

where Δh denotes the specific enthalpy change and Δh_{is} follows the same definition as (3.32).

With the provided data for turbine efficiency, the specific enthalpy change Δh can be calculated as

$$\Delta h = \Delta h_{is}\eta_t = c_{p_{exh}} T_{em}\left(1 - \frac{1}{\Pi_t}^{\frac{\gamma-1}{\gamma}}\right)\eta_t \tag{3.36}$$

Furthermore, Hadef et al. (2012) also made assumption of TFP and Δh that the relation between them is linear. This linear relationship can be expressed as

$$\Delta h = a(\omega_t)TFP + b(\omega_t) \tag{3.37}$$

in which a is the slope and b is the y-intercept, their values depend on the turbine speed ω_t. Here Hadef et al. (2012) suggests that the parameters a and b should be estimated using extrapolated TFP from a model instead of the manufacturer's data. Then the parameter identification for each speed can be done with trivial linear least square method.

In order to benefit the robustness of extrapolation, Hadef et al. (2012) introduced extra data points for $a(0)$ and $b(0)$. Namely

$$a(0) = 0, \quad b(0) = 0$$

The hypothesis is formed due to the fact that during standstill the turbine speed is zero, no energy has been exchanged thus the specific enthalpy change Δh remains zero.

For interpolation and extrapolation of turbine efficiencies that are excluded from the manufacturer's map one can interpolate and extrapolate $a(\omega_t)$ and $b(\omega_t)$ with linear or spline approach. Then (3.37) and (3.35) can be used consecutively with the newly acquired a and b values to compute the turbine efficiencies.

3.3 Validation Methodology for Compressor and Turbo Speed Models

The simulation model for the whole engine needs to be validated against the measurement data to ensure the reliability of simulation-aided controller design. A turbocharged engine can sometimes be seen as a closed loop system when the exhaust gas flow can directly affect intake conditions.

In the engine simulation model, mass flow through the wastegate is described by orifice compressible restriction flow model which has some model errors. The model errors occurred due to the fact that the wastegate position measurements were originally unavailable from the engine test cell. The wastegate flow model had to be parametrised according to the vacuum actuator duty cycle which is less linear to the position. Errors in the wastegate orifice model is unwanted as it causes incorrect calculation of turbine mass flow. The errors may then propagate through estimation of turbine efficiency and affect turbo speed and compressor air flow.

At the point where the simulation quality of the whole engine is reduced by only one component model, it may become difficult to locate and correct other models errors such as temperatures and pressures along the mass flow through the engine. To address this problem and improve the engine model during steady-states, Andersson (2005) suggested a test-bench method for validation and identification of model errors.

The test-bench uses a simple PI-controller to ensure the turbo speed produced by the simulation model is in compliance with measured turbo speed by interacting with the existing wastegate model. The test-bench also controls the throttle model with another PI-controller to ensure correct air flow input to the whole simulation model.

With turbo speed and air flow being fixed to correct values, if the throttle control signals used by the test-bench differ from the actual control signals from measurement data, the models along the air intake needs to be checked. On the other hand after models along the air intake have been corrected, if the models along the exhaust flow still show anomaly, then those models also need to be checked.

3.4 Electric Wastegate Actuator Modelling

In Glad and Ljung (2012) the electric motor that drives the actuator is described with the transfer function

$$G_{motor}(s) = \frac{K_{motor}}{(sT_{motor} + 1)s} e^{-sL_{motor}} \tag{3.38}$$

where K_{motor} is the static gain, T_{motor} the time constant and L_{motor} is the time delay. The transfer function describes how the end position of the actuator is produced by the input PWM signal. The dynamic of the actuator motor is assumed

linear. The backlash effect in the built-in gearbox is regarded small and negligible. The speed of the motor is given by $\frac{K_{motor}}{sT_{motor}+1}$, and $\frac{1}{s}$ accumulates the speeds to positions. In other words, the electric power from the PWM signal generates torque that drives the motor shaft, making the positions to accumulate. When the input signal stops, the actuator will be slowed down by friction and eventually comes to a stop.

As the electric motor is a natural integrator, a better way to design the step-response tests is to send square pulses into the motor instead of steps. When a step is sent through the PWM signal, it changes the speed of the motor, however the position still accumulates and the end effector may be driven into the hard-stops. By using a square pulse with a proper amplitude and duration, one can capture the dynamics during acceleration and deceleration without hitting the hard-stops.

After a number of measurements have been conducted with square pulses in different durations and amplitudes. K_{motor} and T_{motor} are identified with the use of System Identification Toolbox in MATLAB^{TM} software. The identified system is then tested with cross-validation, i.e. to validate with a dataset that has never been used during estimation. The validation data contains measurements where a combination of square pulses were used as input signal.

The fitness of estimated model to the measurement data is measured by normalised root-mean-square deviation method

$$fit = 100\left(1 - \frac{\|y - \hat{y}\|}{\|y - \bar{y}\|}\right) \tag{3.39}$$

where y is the validation data and $\hat{y}$ is the model output. The identified transfer function is then used to build the simulation motor in SIMULINK^{TM}. The noise properties in terms of noise power and variance are also identified from the stand still measurement in order to simulate the effect of measurement noises.

4

Control Theory

In this chapter the theories behind the controller for the boost pressure are presented. Most of the fundamental control strategies are based on the linear assumption of the system that is to be controlled. A linear system shall follow the superposition principle, which is explainined by Glad and Ljung (2014) as: if the inputs u_1 and u_2 lead to the outputs y_1 and y_2, then input $\alpha u_1 + \beta u_2$ would give $\alpha y_1 + \beta y_2$ for any real α and β. The compliance of superposition principle needs to be tested prior the design of the controller, so that nonlinearities can be detected and dealt with beforehand.

4.1 Control Structure

The controller is supposed to deliver the requested boost pressure with the wastegate actuator. Sensors that the controller can use is presented in Table 4.1. Turbo

Table 4.1: *Table with the sensors available for the controller.*

Name	Description
wg_{pos}	Wastegate position
ω_{tc}	Turbo speed
$\dot{m}$	Intake mass flow
p_{amb}	Ambient pressure
T_{amb}	Ambient temperature
p_{ic}	Boost pressure

speed sensor is usually not used to control the boost pressure and the hypothesis is that the feedback of the turbo speed could give a faster and more accurate control. Challenges for the controller design are therefore to make use of the

faster feedback from the turbo speed sensor. The controller design in this thesis is cascade control, described in Enqvist et al. (2014). This design will divide the control problem into two different components: one controller that handles the turbo speed and another that controls the boost pressure. In Figure 4.1 the cascade control structure is shown. The controller's set point is in boost pressure but this will be converted to a set point for the turbo speed with the use of $f_1(\cdot)$ that is described in Section 4.2, this will give the controller a goal for the turbo speed. Model errors in the set point for the turbo speed will be compensated with a controller that uses the feedback from the boost pressure sensor. The correction for these model errors is the output from $F_{boost}(s)$ in Figure 4.1 this controller is described in Section 4.3. $S_{speed}(s)$ is the closed loop for the controller that handles the turbo speed and are described in Section 4.4. $G_{boost}(s)$ is the transfer function from a turbo speed to boost pressure, model identification of this system is described in Section 4.3.

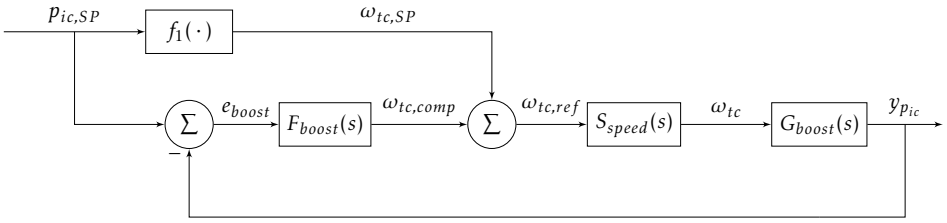

Figure 4.1: *Overview of the controller structure, as can be seen it is a cascade control design that consist of 2 controllers. $f_1(\cdot)$ is the conversion from a boost pressure set point to turbo speed set point. $F_{boost}(s)$ is the controller that will prevent a stationary error for the boost pressure and $\omega_{tc,comp}$ is its compensating term. $S_{speed}(s)$ is the closed loop system for the controller that handles the turbo speed and $G_{boost}(s)$ is the transfer function from a turbo speed to a boost pressure.*

4.2 Calculation of Set Point for Turbo Speed

In this section, three different models to interpret a boost pressure as turbo speed is presented. For simplicity the pressure drop over the intercooler is neglected which gives that the boost pressure is equal to the pressure after the compressor. The models in this section represents the block $f_1(\cdot)$ in Figure 4.1. Because turbo speed physical is measured earlier than the boost pressure it is of importance to receive a turbo speed set point from the set point for the boost pressure.

4.2.1 Physical Modelling

The centrifugal compressor is the compressor commonly used in the automotive turbochargers. In Figure 4.2 a simple centrifugal compressor is illustrated. The impeller transfers mechanical energy from the turbine to the air by accelerating it. As the gas exits it is transported through a diffuser where a controlled deceleration takes place and converts the kinetic energy to static pressure.

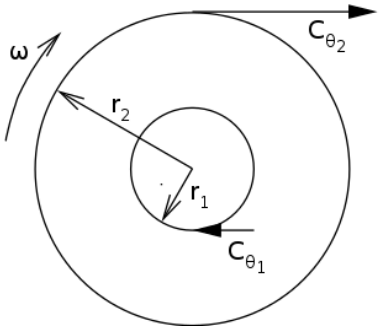

Figure 4.2: *Simple sketch of a centrifugal compressor where the air enters at the eye with tangential velocity, $C_{\theta 1}$, and exits with tangential velocity $C_{\theta 2}$. The compressor's inlet radius is, r_1, tip radius, r_2, and the compressor has an angular velocity, ω. Source: Modeling and Control of Engines and Drivelines, Figure 8.11, page 234. Reproduced with permission from Lars Eriksson.*

An adiabatic compression process is a process that goes from one state to another with no heat exchange, only through work. The energy transfer from the turbine is through work and therefore the process describes the minimum amount of work that is required to go from a state with pressure p_1 and temperature T_1 to pressure p_2. The specific energy change for an adiabatic compression process is given by

$$\Delta h_0 = c_p T_1 \left(\Pi_c^{\frac{\gamma-1}{\gamma}} - 1 \right), \quad \Pi_c = \frac{p_2}{p_1} \tag{4.1}$$

where γ is the ratio of specific heat for air. In the real case the energy transfer from the compressor to the air flow is not optimal. The energy losses are divided

into incidence losses that comes from that the flow does not have the optimal direction relative the impeller blade and friction losses that originates from wall frictions around the flow. Δh_0 is therefore given by subtracting the losses from the actual specific energy input from the turbine, hence

$$\Delta h_0 = \Delta h_t - \Delta h_{losses}, \qquad \Delta h_{losses} = \Delta h_{friction} + \Delta h_{incidence} \tag{4.2}$$

where Δh_t is the specific energy input from the compressor and Δh_{losses} is the specific energy lost to friction and incidence. In Eriksson and Nielsen (2014) it is shown with the use of Euler turbine equation that the general equation for the specific work that has to be supplied is

$$\Delta h_t = \omega(r_2 C_{\theta 2} - r_1 C_{\theta 1}) \tag{4.3}$$

and if the assumption $r_2 C_{\theta 2} >> r_1 C_{\theta 1}$ is made it can be reduced to

$$\Delta h_t \approx \omega r_2 C_{\theta 2} = U_2 C_{\theta 2} \tag{4.4}$$

where U_2 is the rotor tip speed. The only restriction is the assumption that it is a one-dimensional flow.

As mentioned in Eriksson and Nielsen (2014), friction losses, $\Delta h_{friction}$, can be grouped into friction losses that comes from the inlet casing, impeller, diffuser, and collector. In this case as a first approximation the model for the friction losses assumes that it is proportional to the quadratic mass flow as it is for normal turbulent pipe flow as described in Eriksson and Nielsen (2014). The model for friction losses become

$$\Delta h_{friction} = c_1 \dot{m}_c^2 \tag{4.5}$$

Figure 4.3 describes the notations for the incidence losses. In Eriksson and Nielsen (2014) the assumption is that the kinetic energy loss come from the destruction of W_{θ_1} and as the flow is adapted to the blade direction the incidence losses are given by

$$\Delta h_{incidence} = \frac{1}{2} W_{\theta_1}^2 \tag{4.6}$$

Assuming the ideal case that the inlet has no pre-whirl, $C_{\theta_1} = 0$, gives $C_{x_1} = C_1$. Furthermore C_1 is given from the continuity equation

$$C_1 = \frac{\dot{m}_c}{\rho_1 A_1} \tag{4.7}$$

where A_1 is the inlet cross-sectional area and ρ_1 is the inlet static density. With these assumptions and with the use of geometry it is shown in Eriksson and Nielsen (2014) that the incidence losses can be written as

$$\Delta h_{incidence} = \frac{1}{2}\left(U_1^2 - 2U_1 \frac{\dot{m}_c}{\rho_1 A_1} \cot(\beta_{opt}) + \left(\frac{\dot{m}_c}{\rho_1 A_1} \right)^2 \cot^2(\beta_{opt}) \right) \tag{4.8}$$

Assuming that there is no back-sweep, $\beta_{2b} = 90°$. The supplied specific energy is given by (4.4) and becomes

$$\Delta h_t = U_2^2 \tag{4.9}$$

Recognising that

$$U_1 = \omega r_1 \quad \Rightarrow \quad \omega = \frac{U_1}{r_1} \qquad\qquad U_2 = \omega r_2 \quad \Rightarrow \quad \omega = \frac{U_2}{r_2}$$

gives

$$\frac{U_1}{r_1} = \frac{U_2}{r_2} \quad \Rightarrow \quad U_1 = \frac{r_1}{r_2} U_2 \tag{4.10}$$

Inserting (4.5), (4.8), (4.9) and (4.10) into (4.2) with regrouping of some constants it can be written as

$$\Delta h_0 = \frac{k_1}{\rho} U_2^2 + \frac{k_2}{\rho} \dot{m}_c U_2 + \frac{k_3}{\rho} \dot{m}_c^2 \tag{4.11}$$

where k_i are not constants but will have a tip speed dependency but in the model they will be seen as tuning parameters. ρ is the inlet static density. Combining (4.1) and (4.11) and with the use of angular velocity with new regrouping it can be rewritten as

$$c_p T_1 \left(\Pi_c^{\frac{\gamma-1}{\gamma}} - 1 \right) = \frac{c_1}{\rho} \omega^2 + \frac{c_2}{\rho} \dot{m}_c \omega + \frac{c_3}{\rho} \dot{m}_c^2 \tag{4.12}$$

$$U_2 = \omega r_2, \qquad\qquad \omega = 2\pi N$$

where N is rotations per second for the turbine and c_i are the new tuning constants. Solving for ω gives

$$\omega = -\frac{c_2}{2c_1} \dot{m}_c + \sqrt{\left(\frac{c_2}{2c_1} \dot{m}_c \right)^2 - \frac{c_3 \dot{m}_c^2 - \rho_1 c_p T_1 \left(\Pi_c^{\frac{\gamma-1}{\gamma}} - 1 \right)}{c_1}} \tag{4.13}$$

with the conditions

$$\omega \geq 0$$

$$\frac{c_3 \dot{m}_c^2 - \rho_1 c_p T_1 \left(\Pi_c^{\frac{\gamma-1}{\gamma}} - 1 \right)}{c_1} \leq 0$$

Equation (4.13) with knowledge of the set points for the pressure ratio, Π_c, and mass flow, $\dot{m}_c$, during the operating conditions with inlet static density, ρ, and

temperature before the compressor, T_1, a set point for the turbo speed can be calculated.

The advantages with this method are that the only thing needed to calculate the set point for the turbo speed is the set points for $\dot{m}_c$ and Π_c. ρ_1 and T_1 can be seen as ambient conditions with much slower dynamics than the turbo speed and no set point for these are needed. In a control system it is only needed to be implemented as a formula. Drawbacks for this method are that the parameters c_1, c_2, and c_3 need to be estimated. Compressor maps often have very few data points and it is not possible to use corrected quantities for the parameters estimation because the energy term does not handle corrected quantities. Because of this extended measurements with the engine running are needed to be able to estimate the parameters.

4.2.2 Interpolation and Extrapolation of the Compressor Map as Look-up Table

The first approach with the compressor map is to interpolate and extrapolate it and use it as a look-up table. This would give a look-up table that is described by

$$\omega = 2\pi \times \text{MAP}\left(\frac{p_{02,SP}}{p_{01}}, \dot{m}_{c,SP}\right) \tag{4.14}$$

where $p_{02,SP}$ is the set point for the boost pressure before the intercooler. p_{01} is the pressure before the compressor and $\dot{m}_{c,SP}$ is the set point for the mass flow through the compressor. To interpolate the compressor map the extended ellipse model described in Section 3.1.1 is used. Figure 4.4 shows the compressor map with its speed lines and Figure 4.6 is the interpolated surface used as a look-up table. The look-up table is validated with the compressor map data as input, the relative error is presented in Figure 4.7. As seen the relative error is small for all turbo speeds when the map itself is used.

The advantages with this method is that it is very easy to calculate the look-up table. The drawbacks for this method are that the compressor map needs to describe the compressor well to give a good approximation. A look-up table also need memory resources to be implemented and a search algorithm is needed where the search time depend on the number of elements in the look-up table.

4.2.3 Curve Fitting of the Zero-Slope

Another approach is to see if the compressor usually operates in a certain area of the compressor map and then maybe be able to approximate a function for the turbo speed in this area. From the physical modelling described in Section 4.2.1 and in equation (4.12) it is seen that the pressure ratio is a function of mass flow and turbo speed. In Eriksson et al. (2016) it is seen that for tip in and tip out transients the compressor operates around what is called the zero-slope line. The zero-slope line are the points of each speed line that have zero slope. Therefore this is usually the points where the pressure ratio, Π_c, is the maximum for each turbo speed and lies near the surge line. In Figures 4.4 and 4.5 the zero-slope is

the green line with the use of existing points in the compressor map. In Eriksson et al. (2016) a curve fit between normalised pressure ratio at the zero-slope line and turbo speed for 305 different compressors is performed and it shows a very good relation. The relation shown in Eriksson et al. (2016) is described by

$$\frac{\Pi_Z - 1}{\Pi_{c,max} - 1} = N_{c,norm}^{2.29}, \quad N_{c,norm} = \frac{N_{co}}{N_{max,map}} \tag{4.15}$$

where Π_Z is the zero slope pressure ratio which in this case would be the set point for the pressure ratio. $\Pi_{c,max}$ is the maximum pressure ratio in the compressor map. N_{co} is the corrected turbo speed in RPS and $N_{max,map}$ is the maximum turbo speed in the compressor map. Solving for N_{co} gives

$$N_{co} = N_{max,map}\left(\frac{\Pi_Z - 1}{\Pi_{c,max} - 1}\right)^{\frac{1}{2.29}} \tag{4.16}$$

$$\omega = 2\pi N_{co} \tag{4.17}$$

Applying (4.15) on the two compressor maps available in this thesis it is seen in Figure 4.8 that the curve fit also applies to these compressor maps. The advantages with this method is that it is very easy to implement and no estimation of parameters are needed. Maximum turbo speed and maximum pressure ratio are the only needed values from the compressor map. Implementation in a control system is only done with a formula described by equation (4.16). The only needed set point for calculation is the boost pressure and the set point for mass flow is not needed as it is for the other methods described above. The drawbacks with this method is that it will only give a good approximation for set points around the zero-slope line. Recognising that the zero-slope line is the highest pressure ratio for a certain turbo speed and therefore the lowest turbo speed for a certain pressure ratio. This gives that the method should not overestimate the set point for the turbo speed and risk surge. If a set point with high mass flows near the choke line to the right in the compressor map is demanded the set point will probably start at the zero-slope line and move to the right in the compressor map with the help of the controller.

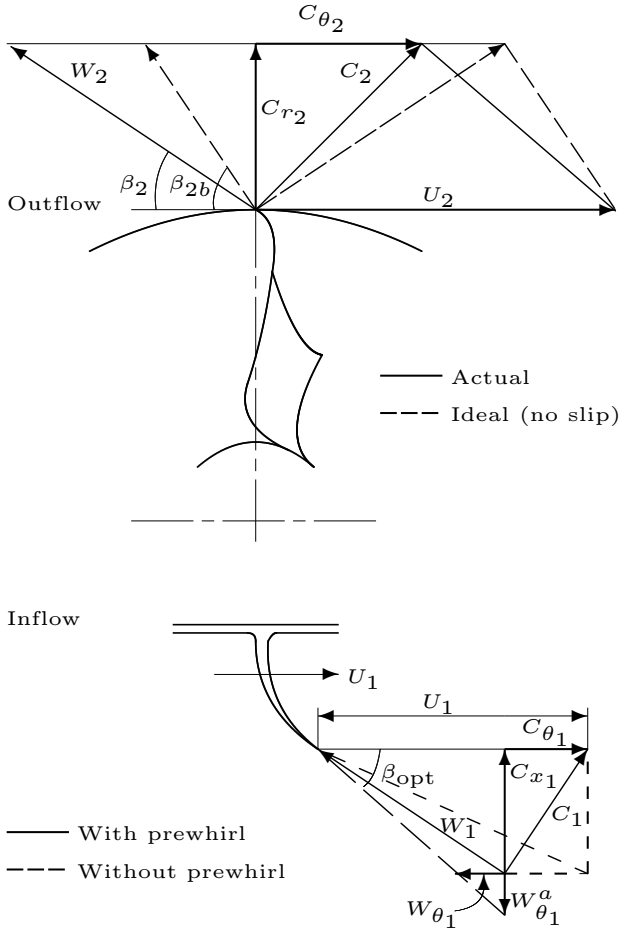

Figure 4.3: *Velocity triangles for the compressor. The flow enters at the eye (inflow) with absolute velocity C_1, with its axial and tangential components denoted C_{x_1} and C_{θ_1}. U_1 is the inlet blade speed. W_1 is the flow velocity relative to the inducer blade with its axial and tangential components denoted $W^a_{\theta_1}$ and W_{θ_1}. Optimal direction of W_1 is when it has the angle β_{opt} to C_{θ_1}. The flow exits at the tip (outflow) with absolute velocity C_2 and its radial and tangential components C_{r_2} and C_{θ_2}. The tip blade speed is U_2 and W_2 is the velocity of the gas relative to the blade. Ideally W_2 would be directed with the angle β_{2b} called back-sweep angle, but because of slip it will be directed in the direction of β_2. Source: Modeling and Control of Engines and Drivelines, Figure 8.12, page 235. Reproduced with permission from Lars Eriksson.*

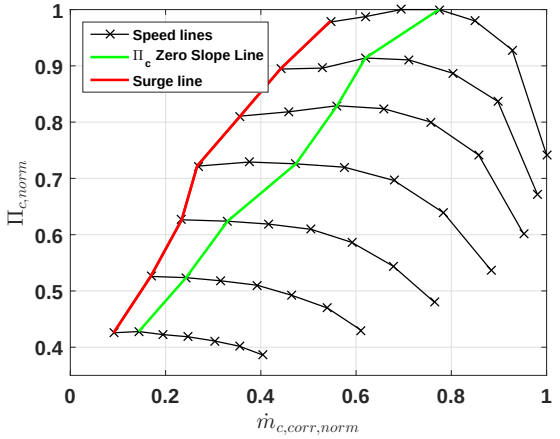

Figure 4.4: *Compressor map for compressor 1, the axis is normalised with the maximum mass flow and pressure ratio. Red line is the surge line, green line is the zero-slop line identified with the points given in the map and the black lines are the speed lines.*

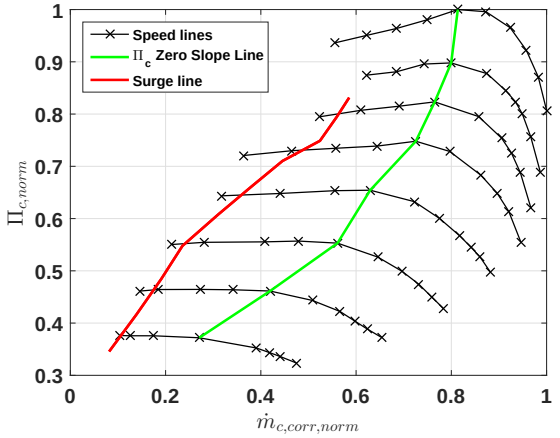

Figure 4.5: *Compressor map for compressor 2, the axis is normalised with the maximum mass flow and pressure ratio. Red line is the surge line, green line is the zero-slop line identified with the points given in the map and the black lines are the speed lines.*

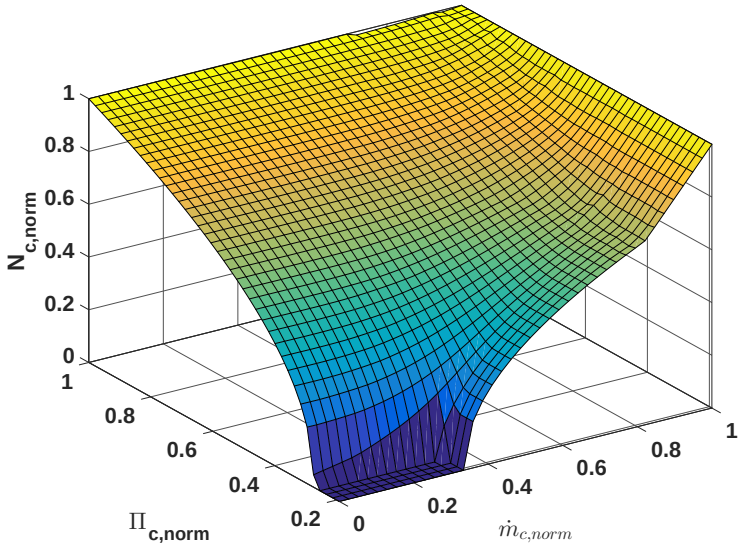

Figure 4.6: *Interpolated look-up table of the compressor map presented as a surface. Important thing here is that it does not have sharp edges and is a smooth surface. Otherwise it could create a problem when interpolating. All axes are normalised.*

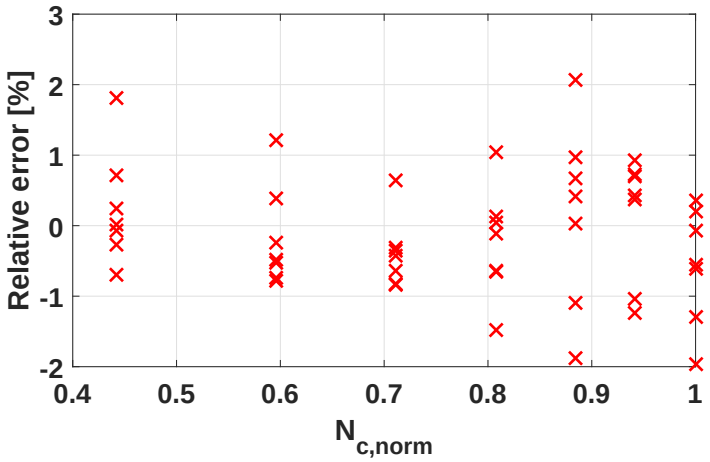

Figure 4.7: *Relative error for the approximated turbo speed using look-up table with compressor map as input. As can be seen the relative error does not seem to vary with turbo speed. The turbo speed is normalised.*

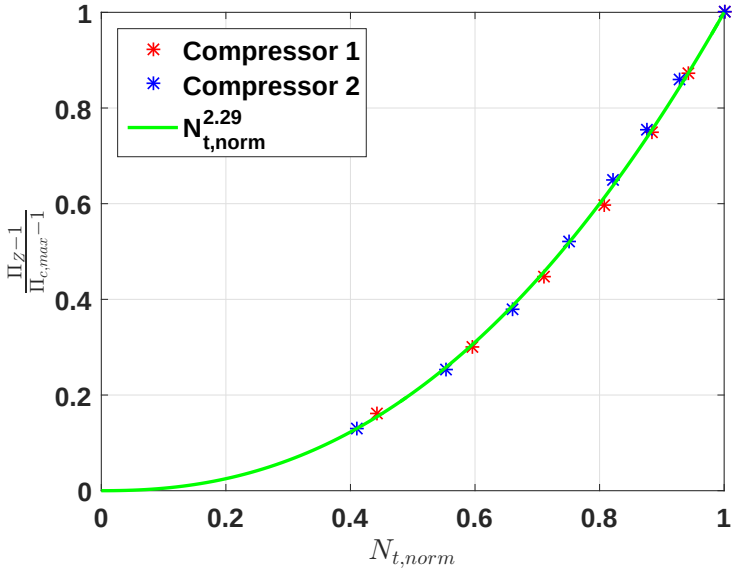

Figure 4.8: *Green line is the curve fit described in Eriksson et al. (2016). Red stars are zero-slope points for compressor 1 and blue stars zero-slope points for compressor 2. The curve fit shows good approximation for the two maps. The only values used from the compressor map is the maximum pressure ratio and turbo speed for the normalisation.*

4.3 Eliminating Static Errors in Boost Pressure

In this section the design of the controller $F_{boost}(s)$ in Figure 4.1 will be described. The goal for the controller is mainly to compensate for the model errors in the feed forward models described in Section 4.2.

4.3.1 Estimation of Transfer Function from Turbo Speed to Boost Pressure

In Figure 4.1 $S_{speed}(s)$ is the closed loop system for the control of the turbo speed and $G_{boost}(s)$ is the transfer function for turbo speed to boost pressure. Challenges with the estimation of $G_{boost}(s)$ is that the input turbo speed can not be controlled directly which means that the turbo speed needs to be controlled through the wastegate controller. Because of this the turbo speed input will be filtered through the system from a wastegate position to turbo speed shown as $G_{speed}(s)$ in Figure 4.9. A problem with this is that it can be hard to excite the system $G_{boost}(s)$ enough. Two approaches for this has been chosen.

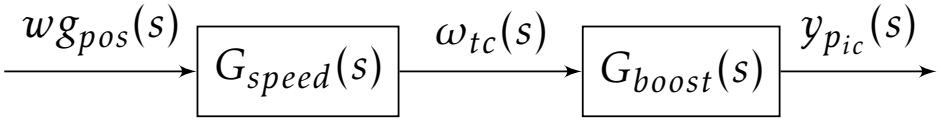

Figure 4.9: *Overview of the system from wastegate position, wg_{pos}, to boost pressure, $y_{p_{ic}}$. Where $G_{speed}(s)$ describes the transfer from wastegate position to turbo speed, ω_{tc}, and $G_{boost}(s)$ describes the transfer from turbo speed to boost pressure.*

Identification of Time Constants

This approach is to perform step-response tests in wastegate position and measure the boost pressure and turbo speed. The system is shown in Figure 4.9. The systems $G_{boost}(s)$ and $G_{speed}(s)$ is assumed to be first order systems described by

$$G_{speed}(s) = \frac{K_1}{1 + T_1 s} \tag{4.18}$$

$$G_{boost}(s) = \frac{K_2}{1 + T_2 s} \tag{4.19}$$

where K_1 and K_2 are the static gains and T_1 and T_2 are the time constants. Combining (4.18) and (4.19) gives the following system descriptions

$$\omega_{tc}(s) = G_{speed}(s) wg_{pos}(s) \quad \Rightarrow \quad \omega_{tc}(s) = \frac{K_1}{1 + T_1 s} wg_{pos}(s) \tag{4.20}$$

$$y_{p_{ic}}(s) = G_{boost}(s) G_{speed}(s) wg_{pos}(s) \quad \Rightarrow \quad y_{p_{ic}}(s) = \frac{K_2 K_1}{(1 + T_2 s)(1 + T_1 s)} wg_{pos}(s) \tag{4.21}$$

This way $G_{speed}(s)$ could be estimated separately and then eliminated from (4.21) under the assumption that it will be possible to identify the same pole in both systems. The static gains will vary with different operating conditions but they can be identified for each step during the processing of the data.

Identification of Time Constants Using Turbo Speed as Input

The second approach is to use the turbo speed measurements as input to estimate $G_{boost}(s)$ in (4.19). The methods described in Section 4.2 could be used to interpret the turbo speed input as boost pressure input but they need to be solved for boost pressure. Because of this the input would consist of measurement error and model error so that the calculated input would be described by

$$p_{ic,input}(\omega_{tc}) = f(\omega_{tc}) + \epsilon_{measurement} + \epsilon_{model} \tag{4.22}$$

where $p_{ic,input}$ is the modelled boost pressure input which consists of: modelled boost pressure $f(\omega_{tc})$, measurement error $\epsilon_{measurement}$, and model error ϵ_{model}. $f(\omega_{tc})$ is applied as a function that uses a method from Section 4.2 to determine boost pressure from turbo speed. $p_{ic,input}(\omega_{tc})$ is then used as true input to the system. The system that awaits identification becomes

$$G_{boost}(s) = \frac{p_{ic,input}(\omega_{tc})}{1 + T_2 s} \tag{4.23}$$

4.3.2 Design of Boost Pressure Controller

The boost pressure controller that is described and chosen in Section 4.1 to be of a cascade control structure the outer loop controller $F_{boost}(s)$ in Figure 4.1 controller goal is to eliminate the static error in boost pressure. Because of this the speed for $F_{boost}(s)$ is not the highest priority but elimination of the static error is, the inner loop $S_{speed}(s)$ in Figure 4.1 is taking care of the controller speed. This gives options in the design of $F_{boost}(s)$ where two approaches is of interest.

Model Based Design

First approach is to use an estimated transfer function described in Section 4.3.1 and use that to parametrise the controller as an IMC described in Enqvist et al. (2014) which gives

$$F_{boost}(s) = \frac{Q(s)}{1 - Q(s)S_{speed}(s)G_{boost}(s)} \tag{4.24}$$

where the transfer function $Q(s)$ is a design parameter that could be chosen to be

$$Q(s) = \frac{1}{S_{speed}(s)G_{boost}(s)(T_c s + 1)} \tag{4.25}$$

where T_c is a design parameter that determine the time constant for the feedback system.

Conditional Integrator

Second approach is to use a conditional integrator and recognising that the biggest disturbances to the system happens with big steps in boost pressure reference. $F_{boost}(s)$ is also only meant to eliminate model errors in the feedforwards described in Section 4.2. The controller $F_{boost}(s)$ can be described by

$$F_{boost}(s) = \begin{cases} 0, & \text{if } u_{wg} = 0 \text{ and } p_{ic} < p_{ic,ref} \\ 0, & \text{if } u_{wg} = 1 \text{ and } p_{ic} > p_{ic,ref} \\ \frac{K_I}{s}, & \text{otherwise} \end{cases} \tag{4.26}$$

where K_I is a design parameter and u_{wg} is the requested wastegate position in $S_{speed}(s)$ that is in the interval of $0 \leq u_{wg} \leq 1$. When $F_{boost}(s)$ is 0 in (4.26) the integrator would also be reset to 0, when this condition is fulfilled it is interpreted as a larger change in the requested turbo speed and an entirely new correction term is to be calculated and it is not depending on the last operation point's correction. For better stability in an implementation the conditions for $F_{boost}(s) = 0$ should hold for a number of consecutive samples before $F_{boost}(s)$ is set to 0 and the integrator is reset. With $F_{boost}(s)$ chosen to be as (4.26) there is no need to estimate a transfer function for $G_{boost}(s)$.

4.4 Turbo Speed Control

As for controlling the turbo speed with wastegate, the compliance of superposition principle can be analysed by step-responses from openly controlled wastegate positions. The result which can be seen in Figure 4.10 shows that the superposition principle is not fulfilled thus the system is nonlinear.

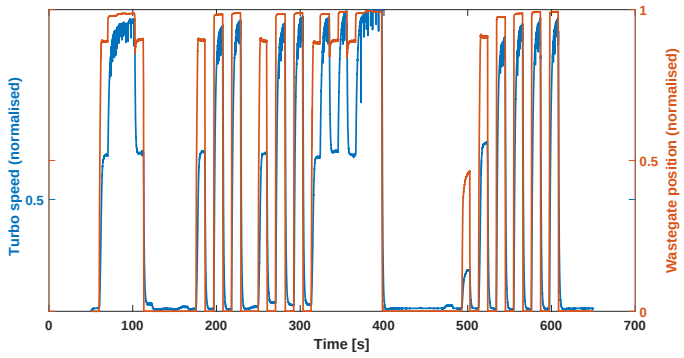

Figure 4.10: *The relationship between wastegate position and turbo speed is non-linear due to unfulfilled superposition principle.*

To design a controller around this nonlinear property of the system several assumptions has been proposed:

- The nonlinearity is contributed by the nonlinear gains during steady state.
- The system follows characteristics of a linear first order dynamic system.
- The time-constant of the dynamic system remain constant.

The suggestion of stationary nonlinear amplitude is mentioned by Enqvist et al. (2014). The procedure is called nonlinear static compensator which is based on the idea that the nonlinearity comes mainly from a nonlinear actuator. A controller that contains such compensator may have the work flow illustrated in Figure 4.11.

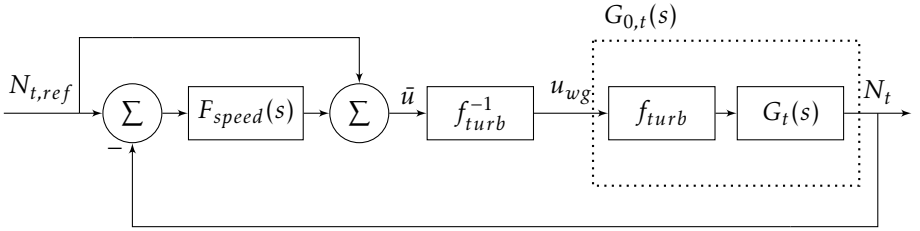

Figure 4.11: *Controller design with nonlinear compensator. $F_{speed}(s)$ is the feedback controller. f_{turb} is the compensator function that models static nonlinearity. f_{turb}^{-1} is the inverse of the function. The system within the dashed lines, $G_{0,t}(s)$, is the approximation of the actual system, in which $G_t(s)$ is treated as a first order dynamic system. The controller output $\bar{u}$ is virtual and is converted to wastegate position demands by f_{turb}^{-1}.*

The controller $F_{speed}(s)$ itself is strictly linear. The output of the controller is virtual and has to be converted to the real control signal through the static inversion of the nonlinear compensator. As Figure 4.11 shows, the inverse of the compensator function f_{turb}^{-1} cancels out the static nonlinearity f_{turb} in the actual system. This allows the controller to interact solely with the linear dynamic system $G_t(s)$.

As the wastegate position is not linear with the turbo speed during steady state, the nonlinear compensator will describe the static relationships between them as

$$N_{t,ss} = f_{turb}(u_{wg}) \Longleftrightarrow u_{wg} = f_{turb}^{-1}(N_{t,ss}) \tag{4.27}$$

The compensator function can either be formulated with physical derivation or with curve-fitting if the amount of measurement data is sufficient. Those methods will be discussed in the upcoming sections.

4.4.1 Nonlinear Static Compensator with Physical Modelling

The nonlinear static compensator expresses the static relationship between a position on the wastegate and a corresponding turbo speed. When combined with a controller the most useful form of the compensator is its inverse, thus the conversion from the virtual control signal to the actual control signal. This is similar to the structure that is commonly used for static feedforward control. The objective of the feedforward is to calculate the set value of the wastegate position given the desired turbo speed and engine mass flow during steady states. The feedforward consists of inverse of equations that describe the steady state relationships among wastegate position, turbo speed, and engine mass flow. The same structure may also serve the purpose for static compensator with the same calculation procedure.

The temperature before the turbine inlet can be described as combination of simple engine-out temperature model and a cooling model in exhaust pipes. The

model structure is suggest by Eriksson and Nielsen (2014) and is given below.

$$T_{em} = T_{amb} + (T_0 + K_t \dot{m}_e - T_{amb}) e^{-\frac{h_{tot} A}{\dot{m}_e c_{p_{exh}}}} \tag{4.28}$$

where $\dot{m}_e$ is the exhaust mass flow; T_{amb} is the ambient temperature; A is the pipe area; $c_{p_{exh}}$ is the specific heat of the exhaust gas. The zero flow temperature from the cylinders T_0 and temperature change rate with flow K_t are constants to be estimated from measurement data. For simplification, the total heat transfer coefficient h_{tot} is also regarded as constant and estimated from measurements.

As Karnik and Jankovic (2012) pointed out the turbine outlet pressure can be approximated to increase quadratically with the exhaust mass flow, which leads to the following assumption and calculation for pressure after turbine, p_t,

$$\dot{m}_e^2 = C_{exh}(p_t - p_{amb}) \Longrightarrow p_t = \frac{\dot{m}_e^2 + C_{exh} p_{amb}}{C_{exh}} \tag{4.29}$$

where p_{amb} is the ambient pressure and C_{exh} is a constant to be estimated from measurement data.

As mentioned in Chapter 3 the turbine efficiency can usually be modelled as functions of turbo speed. With the turbo speed known in this application, information such as pressure ratio can be derived from the efficiency model. However the correctness of the efficiency calculation is often affected by the severe heat losses from the exhaust side of the engine, which leads to that the ideal entropy changes become underestimated. The goal of the calculation is to acquire the pressure ratio across the turbine by using the turbo speed measurement. A simpler curve-fitting model is then developed to fill the gap.

Furthermore it can be observed that during steady state the pressure ratio across the turbine increases exponentially with TSP. This relationship can be described as

$$\Pi_t = C_{\Pi_t} \mathrm{TSP}^k + 1 \tag{4.30}$$

where TSP is given by (3.23). The pressure ratio across the turbine is defined according to (3.21). The fitted curve is tested with three different datasets collected from two turbochargers with different specifications. The result is shown in Figure 4.12.

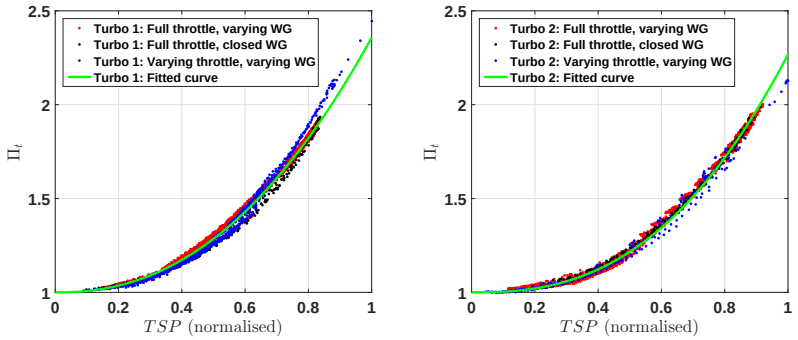

Figure 4.12: *The curve-fitting exponential function of the relationship between TSP and pressure ratio across the turbine. Two different turbochargers were used, with three different datasets each shown in the figures.*

With p_t calculated by (4.29), the exhaust pressure can be obtained by

$$p_{em} = \Pi_t p_t \tag{4.31}$$

TFP can be calculated by (3.26) and the turbine mass flow without correction can then be obtained by (3.22) with p_{em} and T_{em} calculated in (4.28) and (4.31) respectively. The mass flow through the wastegate can be obtained by (3.29). Finally, by following the wastegate orifice model with linear effective area, the wastegate position can be derived by

$$u_{wg} = \frac{\dot{m}_{wg}}{A_{eff,wg} \frac{p_{em}}{\sqrt{R_{exh} T_{em}}} \Psi(\Pi_t)} \tag{4.32}$$

where the definition of $\Psi(\Pi_t)$ is presented in (3.24).

The model is applied on steady-state measurement data with various wastegate positions, and the result is presented in Figure 4.13.

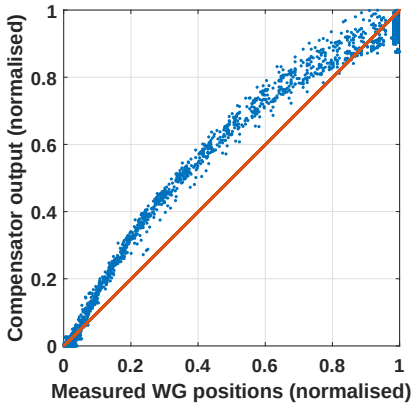

Figure 4.13: *The output of the inverted physical nonlinear compensator function compared with the measured wastegate positions. It can be seen that the calculated positions deviate from measurements as wastegate travels between 10 percent to 80 percent open.*

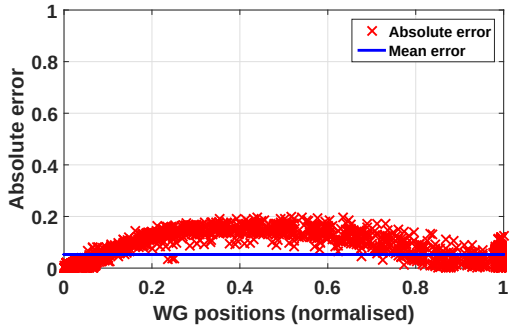

Figure 4.14: *Model errors in the physical compensator function. The errors are presented in absolute as calculations as relative errors would result in division by zero. The mean error lies around 0.05, which corresponds to a uncertainty of 5 percent in positions within the whole travel.*

The physical approach on the compensator function works well within the region where the opening of the wastegate is near close and near open. This holds in terms of model errors as well, which can be seen in Figure 4.14.

The main source of the error is accumulation of model errors during the estimation stages for the above mentioned model equations. The errors that are more significant in the model may impact the correctness of the compensation. For instance when the controller demands a virtual signal to resemble 40 percent opened wastegate, the compensator will interpret as open by 60 percent. This behaviour may affect the performance of the controller.

4.4.2 Development of Nonlinear Static Compensator with Empirical Function

The nonlinear static compensator may also be built by empirical function derived by curve-fitting to measurement data. Although this method decouples most of the physical insights, if the function is accurate, invertible and with simple structure, it will significantly reduce calculation loads.

Assume that the exhaust mass flow is constant, then by gradually closing the wastegate valve the turbo speed will be increasing monotonically. If the position is constant, then the turbo speed will be monotonically increasing with increasing mass flow. With this phenomenon in mind, the empirical function for the compensator will be monotone, which ensures that the function would be invertible with unique solution. To further simplify the structure, assume the fuel injection is perfectly regulated to satisfy the constant ideal air-fuel ratio in the combustion chamber, the variables in the empirical function will be air mass flow, wastegate positions (normalised to between 0 and 1) and turbo speed.

Measurement data is commonly available by holding engine speed constant and varying throttle and wastegate valve which means that the measurement data is not taken with respect to air mass flow. This can be dealt with by interpolating the measurement data with respect to air mass flow such that relationships between wastegate positions and turbo speeds are made available for each unique air mass flow.

To further elaborate the hypothesis, the identification used a steady state measurement dataset with full throttle and varying wastegate positions during a wide range of engine speeds. The identification dataset is acquired from a different engine equipped with a different turbocharger. The measurements and interpolated values are presented in Figure 4.15, with normalised axis.

The proposed empirical function for one constant air mass flow is as follows

$$N_t = ae^{-bu_{wg}} + c \tag{4.33}$$

where a, b, and c are positive real numbers. The wastegate position u_{wg} is normalised between 0 and 1. When the wastegate is fully opened, with this normalisation, the function produces the lowest possible turbo speed $ae^{-b} + c$ due to b is positive. As the wastegate closes, the function produces $a + c$ which represent the highest turbo speed possible for the current mass flow.

This hypothetical proposal is then verified on several interpolated data with different constant mass flow. The result is illustrated in Figure 4.16.

Eventually, the parameters a, b, and c will be functions of air mass flow as the appearance of the curves are formed by the parameters. Hence

$$N_t = a(\dot{m}_a)e^{-b(\dot{m}_a)u_{wg}} + c(\dot{m}_a) \tag{4.34}$$

For each interpolated air mass flow, the parameters a, b, and c are estimated. The estimated parameters are presented in Figure 4.17 with corresponding air mass flow on the x-axis.

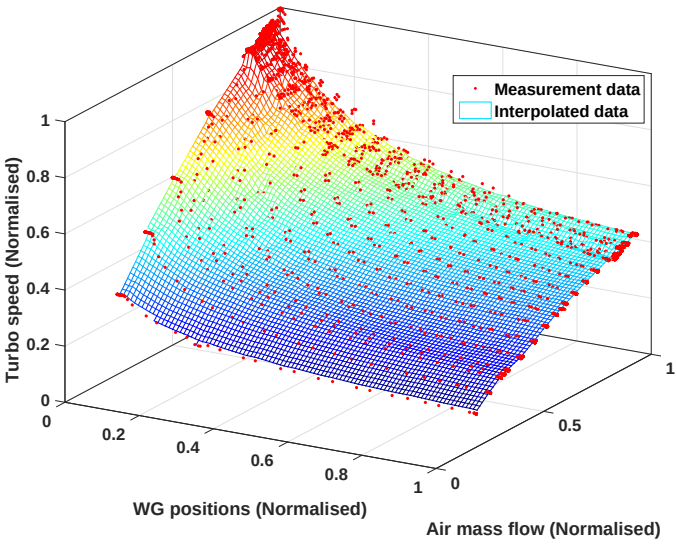

Figure 4.15: *Interpolated measurement data showing relationships among wastegate position, air mass flow, and turbo speed. For each unique air mass flow the turbo speed increases monotonically with the closing of wastegate (position towards zero).*

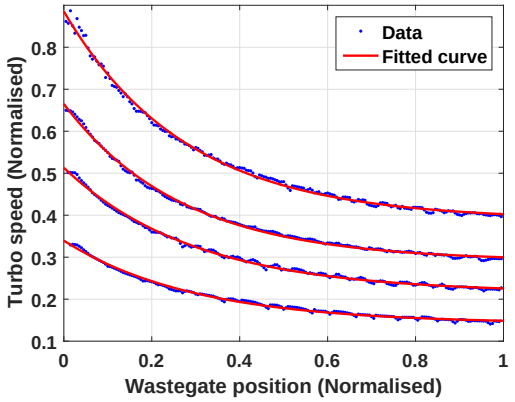

Figure 4.16: *The proposed function structure is tested on a selection of different interpolated data, and the estimated curves fit the data well.*

From Figure 4.17 the parameter a and c increases linearly with air mass flow and parameter b can be seen as constant. The final iteration of the empirical nonlinear static compensator function now has the following form

$$N_t = (a_1 \dot{m}_a + a_2) e^{-b u_{wg}} + c_1 \dot{m}_a + c_2 \tag{4.35}$$

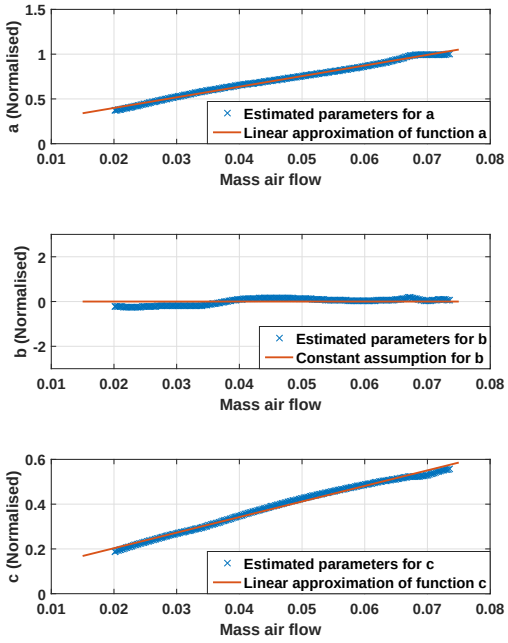

Figure 4.17: *The a, b, and c are estimated and plotted against air mass flow. It is clear that a and c are linear functions of air mass flow while b can be treated as constant. (The a, b, and c parameters in the figure have been normalised and off-setted)*

where a_1, a_2, b, c_1, and c_2 are all constants. The inverse of the function will be

$$u_{wg} = -\frac{1}{b} ln(\frac{N_t - c_1 \dot{m}_a - c_2}{a_1 \dot{m}_a + a_2}) \tag{4.36}$$

which will be used more frequently by the controller.

A comparison with a similar fashion as in Figure 4.13 has been made and is shown in Figure 4.18, and the errors with the curve-fitting approach is shown in Figure 4.19.

The empirical nonlinear static compensator function causes less error than the physical model especially within the region of partially open wastegate. The structure of the function is also simple, as it only requires two signals to calculate the desired variable. The physical approach requires additionally three more measurements: mass fuel injection, ambient temperature, and ambient pressure. The empirical function is also monotone and invertible, makes it more flexible for the controller design.

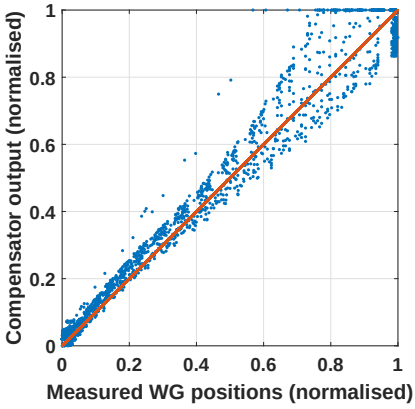

Figure 4.18: *The output of the inverted empirical nonlinear compensator function compared with the measured wastegate positions.*

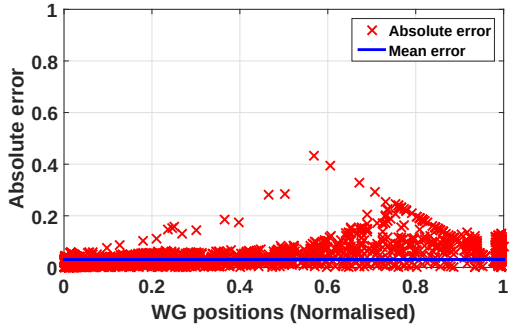

Figure 4.19: *Model errors in the empirical compensator function. The errors are presented in absolute as calculations as relative errors would result in division by zero. The mean error lies around 0.03.*

4.4.3 Turbo Speed Controller

After the static nonlinearities have been dealt with, the rest of the system that needs to be identified is the linear dynamic system. As the nonlinear compensator calculates the static turbo speeds for different wastegate positions, the gain in the linear dynamic system will be one. For instance, if an instant step in the wastegate position produces a change by 5000 Revolutions Per Minute (RPM) in the turbo speed, the compensator function will translate the position change into speed change as a virtual input to the prospective dynamic system, resulting the actual turbo speed to change by 5000 RPM, thus the gain of the dynamic system is one.

For simplicity, the dynamic system is treated as first order. The property that awaits to be identified is the time constant T and possible time delay L of the

system. When T and L become known, the model of the dynamic system that describes how wastegate positions affect turbo speeds becomes

$$G_{0,t} = f_{turb}(u_{wg}, \dot{m}_a)\frac{1}{sT+1}e^{-sL} \tag{4.37}$$

The identification of T and L can be done by performing system identification of process models. The input data is various wastegate positions and should be designed in such way that the input activates all the frequency contents of the system. To perform linear system identification, the wastegate positions will be converted into virtual turbo speed with the nonlinear compensator function. With the measured turbo speeds as system output, the system identification can be performed by using System Identification Toolbox in MATLAB^{TM} software. The time delay term e^{-sL} can be substituted by Padé approximation described in Enqvist et al. (2014)

$$e^{-sL} \approx \frac{1 - sL/2}{1 + sL/2} \tag{4.38}$$

It is mentioned earlier that the inverse compensator function cancels the static nonlinearities in the system, leaving the opportunities for the controller to interact solely with the linear part of the system, hence the identified linear first order dynamic system.

This structure made it appropriate to design a controller based on IMC. With Padé approximation the internal model becomes

$$G(s) = \frac{1 - sL/2}{(sT+1)(1+sL/2)} \tag{4.39}$$

Follow the derivation described in Enqvist et al. (2014) the IMC controller will have the following transfer function

$$F_{speed}(s) = \frac{(1+sL/2)(1+sT)}{s(L + T_c + sT_cL/2)} \tag{4.40}$$

where T_c is the design parameter that represents the desired time constant for the closed system $S_{speed}(s)$ as seen in Figure 4.1. The controller transfer function can also be written as

$$F_{speed}(s) = \frac{T + L/2}{T_c + L}\left(1 + \frac{1}{T + L/2}\frac{1}{s} + \frac{TL}{2(T + L/2)}s\right) \tag{4.41}$$

This can be identified as a PID-controller with the following parameters

$$K_p = \frac{T + L/2}{T_c + L} \qquad T_i = T + L/2 \qquad T_d = \frac{TL}{2(T + L/2)} \tag{4.42}$$

given the PID-controller has the structure

$$F_{PID}(s) = K_p(1 + \frac{1}{T_i}\frac{1}{s} + T_d s) \tag{4.43}$$

If the time delay L is non-existence or negligible, the controller is reduced to a PI-controller

$$K_p = \frac{T}{T_c} \qquad T_i = T \tag{4.44}$$

When the D-part of the controller is indeed required, the measurement signal needs to be filtered in order to avoid derivation of measurement noise. Suggested by Enqvist et al. (2014), this can be done by replacing the D-part with an approximation

$$\frac{T_d s}{\mu T_d s + 1} \tag{4.45}$$

where μ is a design parameter that adjust sensitivity for higher frequencies. When a proper μ is presented, the higher frequencies in s will be damped; noises that contain high frequencies will be suppressed and stuttering in control signals decreases.

The output from the controller is the virtual control signal and needs to be converted to wastegate position through the nonlinear compensator function.

The final implementation of the controller takes place in discrete time. By using backwards Euler method i.e. $s = \frac{z-1}{T_s z}$, the PID-controller (including modified D-part) is discretised as

$$F_{speed}(z) = K_p(1 + \frac{T_s z}{T_i(z-1)} + \frac{T_d(z-1)}{\mu T_d(z-1) + T_s z}) \tag{4.46}$$

where T_s is the sample time and K_p, T_i, T_d are identified as in (4.42).

Another concern is integrator wind-up. As the wastegate positions are limited to between fully closed and fully open, any control signal that demands positions outside the limits has to be saturated. This will eventually make the integrator to wind up. To address the issue, the saturated position is converted with the compensator function, and the difference from the original control signal is substituted from the integrator. The principle sketch of the controller with anti wind-up may be found in Figure 4.20.

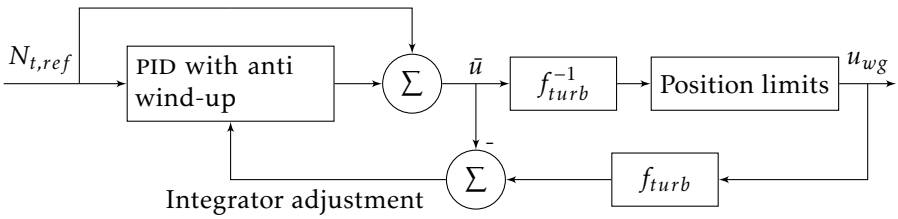

Figure 4.20: *The controller design with anti wind-up. When saturation conditions are reached, the differences across the saturation is then calculated. The saturated position will pass through the compensator function in order to conform the virtual signals from the controller. The converted differences are immediately substituted from the integrator part of the controller.*

4.5 Wastegate Valve Position Control

One of the main purposes of the thesis is to analyse whether it is advantageous to use electrically actuated wastegate valve instead of traditional vacuum actuated ones. This requires a control algorithm for the actuator to be developed. The electric actuator unit has a built-in position sensor. The maximum travel of the actuator's end effector is limited with two hard-stop positions which are approximately 90 degrees apart. Carelessly crashing into these hard-stops may damage the unit, thus it is unsuitable to conduct controller design and tuning directly on the unit. To develop the control algorithm safely and effectively, a model-based approach is chosen and it involves 5 steps:

1. Measure position sensor noise during stand still.
2. Perform step-response tests.
3. Use system identification to find out K_{motor}, T_{motor}, and L_{motor}.
4. Build a simulation motor and conduct controller design.
5. Validate the controller on the actual unit.

The estimated model for the electric motor described by Equation (3.38) is also used for controller design. Enqvist et al. (2014) stated that IMC-based controller design is unsuitable for systems that are unstable. This is true for the actuator motor, as one of the poles in the transfer function lies in origo. A state-feedback controller with observer is then suggested to make use of the estimated model together with the position measurement. The state space representation of the model with time delay ignored is

$$\begin{aligned} \dot{x} &= Ax + Bu \\ y &= Cx \\ x &= \begin{bmatrix} x_1 \\ x_2 \end{bmatrix} \qquad A = \begin{bmatrix} -\frac{1}{T_{motor}} & 0 \\ 1 & 0 \end{bmatrix} \quad B = \begin{bmatrix} \frac{K_{motor}}{T_{motor}} \\ 0 \end{bmatrix} \quad C = \begin{bmatrix} 0 & 1 \end{bmatrix} \end{aligned} \tag{4.47}$$

where x_1 denotes the state for speed and x_2 denotes the state for position. The discrete state space model will also be needed. Zero-order hold assumption is used for simplicity and the discrete model is given by

$$\begin{aligned} x[k+1] &= Fx[k] + Gu[k] \\ y[k] &= Hx[k] \\ x[k] &= \begin{bmatrix} x_1[k] \\ x_2[k] \end{bmatrix} \qquad H = \begin{bmatrix} 0 & 1 \end{bmatrix} \end{aligned} \tag{4.48}$$

F and G are the discrete state space matrices. The calculation of those utilises piecewise constant assumption of model sampling and a one-step computation method for this is presented by Gustafsson (2012) as follows

$$EXPM\left(\begin{bmatrix} AT_s & BT_s \\ 0 & 0 \end{bmatrix}\right) = \begin{bmatrix} F & G \\ 0 & I \end{bmatrix} \tag{4.49}$$

where $EXPM$ stands for matrix exponential. The matrices A and B are given in (4.47), and T_s is the sample time.

4.5.1 State-Feedback Controller

A functioning state-feedback controller requires all states of the system to be known, in this case speed and position. The actuator unit provides only position measurements which implies that an observer is needed to estimate speed state in order to fully take advantage of state-feedback control.

The observer applies discrete Kalman filter approach to ensure quality of the speed estimation. The state-matrices used in the Kalman filter are F, G, and H from (4.48) and (4.49). The noise variances can be acquired from the earlier performed noice measurements. Should the position measurements be filtered beforehand the noise variance will be tuned manually. The measurement and the model error covariance matrix is manually selected to balance between correctness and noise-suppression. The implementation details about discrete Kalman filter is thoroughly described in Gustafsson et al. (2011).

The control signal for state-feedback controller is explained by Glad and Ljung (2012) as

$$u = -Lx + l_0 r \quad L = \begin{bmatrix} l_1 & l_2 \end{bmatrix} \tag{4.50}$$

where r is the control set-point, L is the state-gain and l_0 is a correction term that ensures the static gain of closed system remains 1.

In Glad and Ljung (2012) the optimal choice of L can be formulated as linear quadratic optimisation criteria

$$\begin{aligned} J &= \int_0^\infty (x^T(t)Qx(t) + u^2(t))dt \\ Q &= \begin{bmatrix} q_1 & 0 \\ 0 & q_2 \end{bmatrix} \qquad\qquad x = \begin{bmatrix} x_1 \\ x_2 \end{bmatrix} \end{aligned} \tag{4.51}$$

J is the cost function that will be minimised. The diagonal penalty matrix Q indicates whether if the speed or position that need to react faster; as for the actuator that reaches and holds a position, the latter is desired. x_1 and x_2 are states for speed and position respectively, which means that q_2 shall have greater weight than q_1. The solution u that meets the optimisation of the cost function is

$$u = -Lx = -B^T Px \Longrightarrow L = B^T P \tag{4.52}$$

in which P solves the algebraic Riccati equation

$$Q + A^T P + PA - PBB^T P = 0 \tag{4.53}$$

with A,B, and Q defined in (4.47) and (4.51). The closed system is then

$$G_{motor,c} = C(sI - A + BL)^{-1}B = \frac{\frac{K_{motor}}{T_{motor}}}{s^2 + \frac{K_{motor}l_1+1}{T_{motor}}s + \frac{K_{motor}l_2}{T_{motor}}} \tag{4.54}$$

As seen in (4.54), to ensure the static gain of closed system to be one l_0 will be chosen as equal to l_2, thus

$$u = l_2 r - l_2 y - l_1 \dot{y} = l_2(r - y) - l_1 \dot{y} \tag{4.55}$$

where y is the measured position and $\dot{y}$ is actuator speed estimated by the Kalman observer. This is essentially a PD-controller with l_2 as proportional gain. The D-part functions only on the observer output rather than the error term $r - y$. When the controller is applied on the physical actuator, it is also practical to introduce an integration part to eliminate the static errors. Although the actuator motor itself contains a natural integrator, factors as friction and limited control resolution may still cause static errors if only the state-feedback controller is used. The additional I-controller takes the error term $r - y$ as input and the output is then added together with the state-feedback controller output. The actuator PWM input is finite, meaning that anti wind-up feature is needed. The whole controller design is illustrated in Figure 4.21.

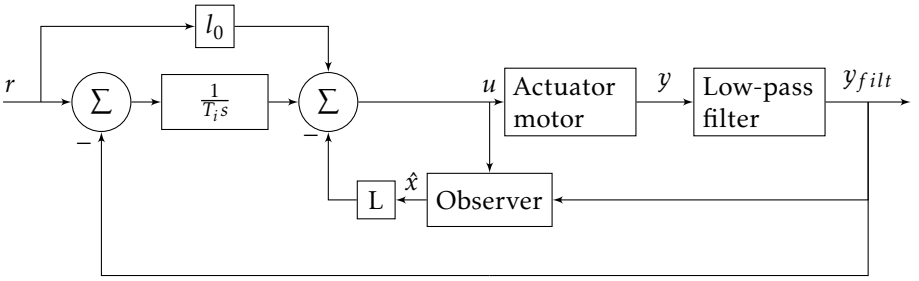

Figure 4.21: *The controller design for the wastegate actuator. The state-feedback control uses observer-estimated states $\hat{x}$. An integrator is also used for correction of static errors. Though absent in the illustration, the prevention of integrator wind-up is required. A digital low-pass filter is applied to avoid overreaction to the possible exhaust gas pulsations.*

4.5.2 Complementary Features

The actuator should not attempt to explicitly cancel the frequency of the exhaust pulsations in order to avoid stability issues in the controller. The issue can be mitigated by passing the position measurement through a low-pass filter as shown in Figure 4.21. The cut-off frequency of the filter is determined by the lowest engine speed after which the wastegate is to be controlled, i.e. not constantly staying fully open. Assume this engine speed is N_e RPM, the cut-off frequency for the low-pass filter is given by

$$f_{cutoff} = 2\frac{N_e - \Delta N_{margin}}{60} = \frac{N_e - \Delta N_{margin}}{30}[Hz] \tag{4.56}$$

where ΔN_{margin} is a design margin that offsets the engine speed to ensure the damping of the pulsation frequency.

After the actuator is installed with a shaft that connects the wastegate valve, the end positions may not be the same as the actuators internal hard-stops. Ni et al. (2013) recommends an auto-find function for the end positions to be implemented so the end positions of the actuator travel is automatically calibrated and remembered. During the calibration the position controller is on standby. The actuator performs an up-sweep and down-sweep in low speed to find the upper bound and lower bound respectively. The identification of the end position can be done by supervising the position derivative, in other words the change rate of position. When the actuator is in motion, the derivatives is non-zero. When the actuator is stuck in end position the derivatives ought to be zero, however due to the presence of measurement noise it is difficult to have a pure series of consecutive zeros to establish a confirmation. The identification can be made robust by using Cumulative SUM (CUSUM) algorithm mentioned in Nyberg and Frisk (2014). CUSUM algorithm is based on the following recursive function

$$T[k] = \max(0, T[k-1] + r[k-1]) \quad T(0) = 0 \tag{4.57}$$

In this application: $r = -1$: position derivative greater than derivative threshold. $r = 1$: position derivative smaller than derivative threshold. The introduction of derivative threshold aims to provide flexibility in the detection. When an end position is reached, the position derivatives will more likely to be considerably smaller than that during motion, leading to increasing $T[k]$. $T[k]$ will then be constantly compared to a threshold value for CUSUM. A confirmation is generated as $T[k]$ exceeds the CUSUM-threshold and the current position is remembered as end position.

As soon as the confirmation for the upper end position is dispatched, the actuator reverts direction and the same method is applied to find the lower end position. When both positions are identified and remembered, the controller proceeds to function normally.

Ni et al. (2013) also suggested to implement soft-landing and tightening functions. With soft-landing the wastegate lands gently when set-point is near end positions. When all the exhaust gas needs to be concentrated on the turbine the tightening function seals the wastegate when fully closed to prevent leakage. The end positions are given by the calibrated values from the auto-find function that runs during initialisation. The tightening function is activated when the set-point is the closing position and the valve is approaching. When the wastegate closes, a constant offset is applied to the actuator PWM signal to reinforce the pressure on the valve. The soft-landing function identifies in advance that the valve moves towards the end positions and narrows the maximum PWM output when the valve is in vicinity of end positions.

4.6 Wastegate Valve Position Disturbance Analysis

In today's automotive turbocharged engines, the wastegte is commonly actuated with PWM signal. As described in Section 2.3 the position of vacuum actuated wastegate is seldom linear to the PWM duty cycle. Due to lack of position measurement in most applications the wastegate position itself is not controlled. The amount of PWM duty cycle to apply is usually calculated directly from boost pressure feedback. As long as the boost pressure is unaffected by local disturbances across the wastegate, the feedback controller will not take any countermeasures to compensate the position errors caused by the disturbances. In this chapter the hypothetical disturbances that affects the wastegate actuator position are presented.

4.6.1 Exhaust Gas Pulsations Effect on Wastegate Valve

The pressure ratio over the wastegate valve results in a mass flow and this flow acts as a force on the wastegate valve. This force can be seen as a disturbance on the wastegate valve which affect its position. If the flow is assumed constant this force would help when opening the wastegate valve and counter-act the change when closing the wastegate valve. A 4-stroke engine cylinder performs one exhaust cycle each other revolution. The ignition timing for the 4-cylinder engine therefore originates to two evenly placed exhaust cycles per revolution. The opening and closing of the exhaust valves are assumed to give rise to pulsations in the exhaust manifold pressure. Because of this pulsation in pressure, the pressure ratio would also pulsate which leads to the disturbance force on the wastegate valve to pulsate. To detect frequency contents in signals the Fast Fourier Transform algorithm is used which uses the Discrete Fourier Transform (DFT), that in (Gustafsson et al., 2011) is defined as

$$\begin{aligned} X[n] &= \sum_{k=0}^{N-1} W_N^{-nk} x[k] \\ W_N &= e^{\frac{2\pi i}{N}} \\ k, n &= 0, ..., N-1 \end{aligned} \tag{4.58}$$

where x is the sampled signal and X is the DFT of x. By calculating the DFT for the measured wastegate position the frequencies exciting the wastegate valve can be detected and therefore also the pulsations affecting the wastegate valve can be visualised and identified.

4.6.2 Frequency Analysis of Vacuum Controlled Actuator for Wastegate

Energy spectrum for a system gives insight of the system's bandwidth as well as resonance frequencies.

For the vacuum controlled actuator the resonance frequencies for the system is of interest when studying pulsations in the wastegate valve position. Insight

of the resonance frequencies would help to determine whether the pulsation frequencies originate from the actuator itself or from conditions in the exhaust manifold.

In general, the response time of a system is connected to the systems bandwidth where a broader bandwidth gives a system with faster response time. This would provide an insight of the actuator's response time for the open system.

In Gustafsson et al. (2011) the energy spectrum for a signal, x, with limited energy is defined as

$$\Phi_{xx}(\omega) = |X(\omega)|^2 \tag{4.59}$$

where $X(\omega)$ is the Fourier Transform of x. This description is for the true spectra and it assumes infinite time, when doing experiments sampling of the signal is done during a time window. To analyse the energy spectrum for a sampled version the periodogram is used. Gustafsson et al. (2011) defines the periodogram to be

$$\hat{\Phi}_N\left(\frac{2\pi n}{NT}\right) = \frac{T}{N}|X[n]|^2 \tag{4.60}$$

where $X[n]$ is the DFT of x as defined in Equation (4.58). T is the sampling time and N is the number of samples. In Ljung and Glad (2004) it is seen that the periodogram has a tendency to be very noisy and it can be hard to interpret resonance frequencies and bandwidth in it. Ljung and Glad (2004) mention different methods to reduce the variance in the periodogram, these methods uses different window functions to smooth the periodogram. Example of these methods are Welchs and Blackman-Tukey.

To estimate the energy spectrum for the wastegate actuator filtered white noise would be used as duty cycle input where the cut-off frequency for the filter would be determined by the Nyquist frequency that is defined as half the sampling frequency for the position sensor.

After the performed frequency analysis, the estimated frequency contents of the wastegte actuator can be compared to the visible frequencies in DFT of measurement data for possible matches.

5

Results and Achievments

In this chapter the results for this thesis are presented.

5.1 Model Validations for Compressor Mass Flow and Efficiency

The estimated basic ellipse model for the compressor mass flow is shown in Figure 5.1. For comparison, the estimated model is plotted together with the speed lines from the manufacturer's performance map. The axis in the figure are normalised with (3.3).

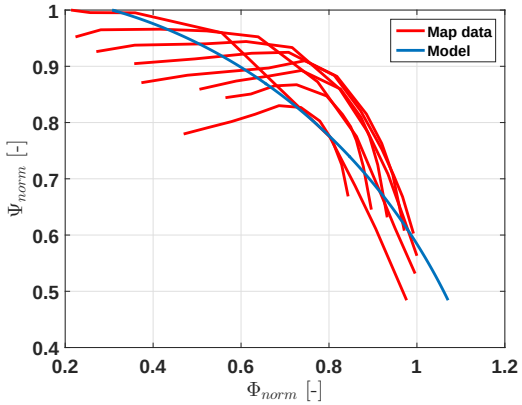

Figure 5.1: *The blue line is the basic ellipse model and the red lines are different speed lines from the performance map. The axis are normalised with* (3.3).

In Figure 5.2 and 5.3 the relative errors of basic ellipse model and extended ellipse model are compared side by side, with relative errors defined in (3.1).

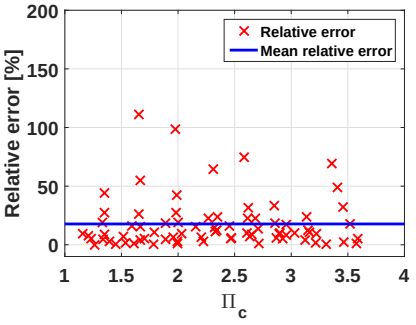

Figure 5.2: *Basic ellipse model, relative error against pressure ratio. Mean error line shows a mean relative error of 17.75 %.*

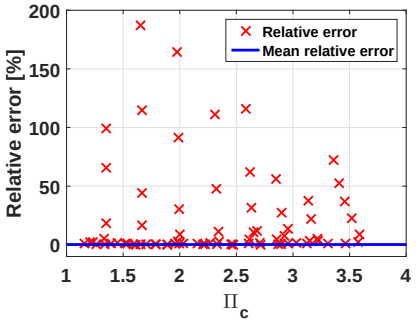

Figure 5.3: *Extended ellipse model, relative error against pressure ratio. Mean error line shows a mean relative error of 0.22 %*

The relative model errors for the compressor efficiency model is shown in Figure 5.4. The model has 2.14 % relative error as a mean.

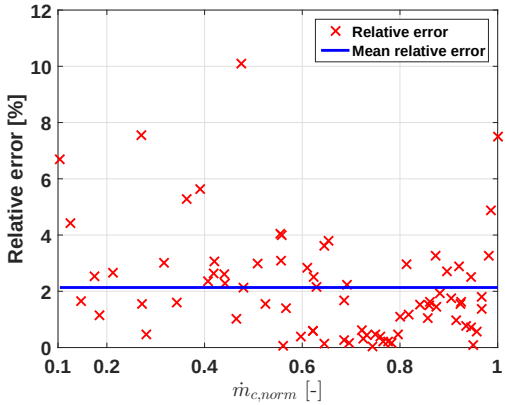

Figure 5.4: *Compressor efficiency model, relative error against normalised compressor mass flow. Mean error line shows a mean relative error of 2.14 %.*

5.2 Model Validations for Turbine Mass Flow

The resulted turbine mass flow model qualities in terms of relative errors for both physical restriction model and non-physical square root model are presented in Figure 5.5 and 5.6.

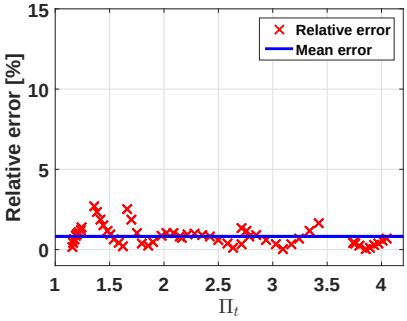

Figure 5.5: *Model evaluation of turbine mass flow physical restriction model with effective area that depends on the pressure ratio and TSP. The mean error of the model is 0.8232 %.*

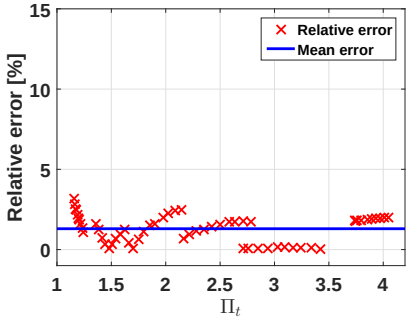

Figure 5.6: *Model evaluation of turbine mass flow non-physical square root model. The mean error of the model is 1.299 %.*

5.3 Model Validations for Turbine Efficiency

The calculated turbine efficiency with BSR model is evaluated and the result in terms of model error is presented in Figure 5.7.

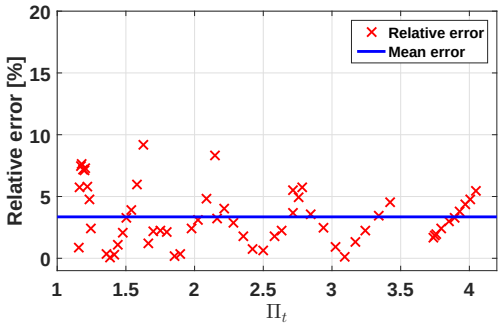

Figure 5.7: *Model evaluation of BSR model for turbine efficiency. The mean error of the model is 3.352 %.*

The evidence for the linear assumption of TFP and Δh suggested by Hadef et al. (2012) can be visualized in Figure 5.8.

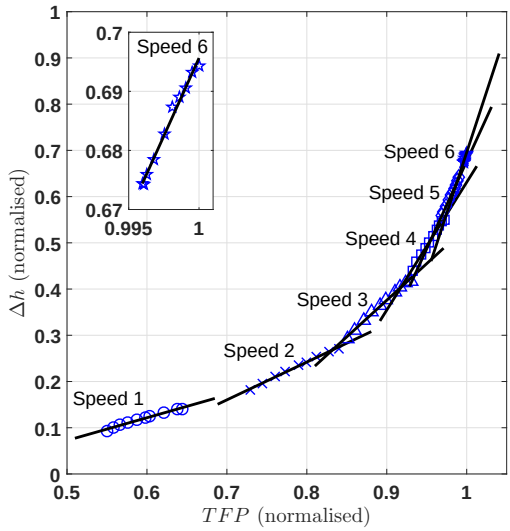

Figure 5.8: *The relationship between TFP and Δh presented with different turbine speeds with enhanced view on the 6^{th} speed. The axis in the figures are normalised with their corresponding maximum values. Each different symbol represent a turbine speed and the increment of the speed numbers follow the increment of mapped turbine speeds. It can be seen than for each speed the specific enthalpy change increases linearly with TFP.*

The resulted a and b from estimating parameters for (3.37) are shown in Figure 5.9. The TFP used during the estimation were calculated by the non-physical square root model given by (3.26).

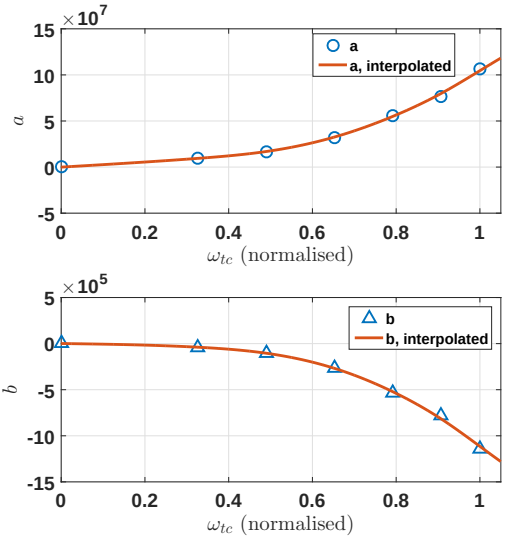

Figure 5.9: *Estimated a and b parameters as functions of turbine speeds with spline interpolation. The x-axis in the figures are turbine speeds normalised with the corresponding maximum value registered in the data map. The zero assumption for $a(0)$ and $b(0)$ is also included.*

The quality of the estimated turbine efficiency model by the approach suggested by Hadef et al. (2012) is shown in Figure 5.10 in terms of model errors. A comparison with BSR model can be found in Figure 5.11.

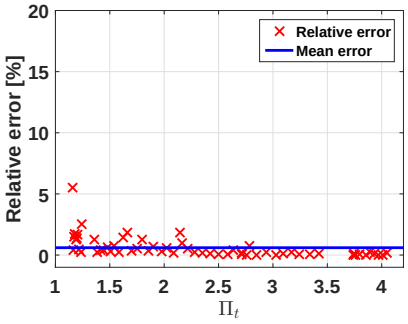

Figure 5.10: *Model evaluation of turbine efficiency model with model structure suggested by Hadef et al. (2012). The mean error of this model is 0.6 %.*

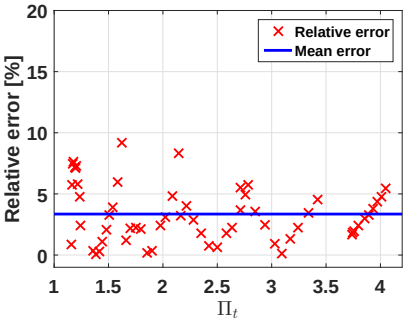

Figure 5.11: *Model evaluation of turbine efficiency model with BSR method with a mean error of 3.352 %.*

5.4 Simulation Model Validation

The validation method described in Section 3.3 is used to check if the updated models for turbine and compressor have shown signs of improvement. To visualise the improvement on the turbine and compressor modelling, a before-after comparison was performed on pressures and temperatures in charged air, exhaust manifold, and after the turbine. The simulation results compared to measurement from the original simulation model and the throttle test-bench signal are shown in Figure 5.12 and Figure 5.13.

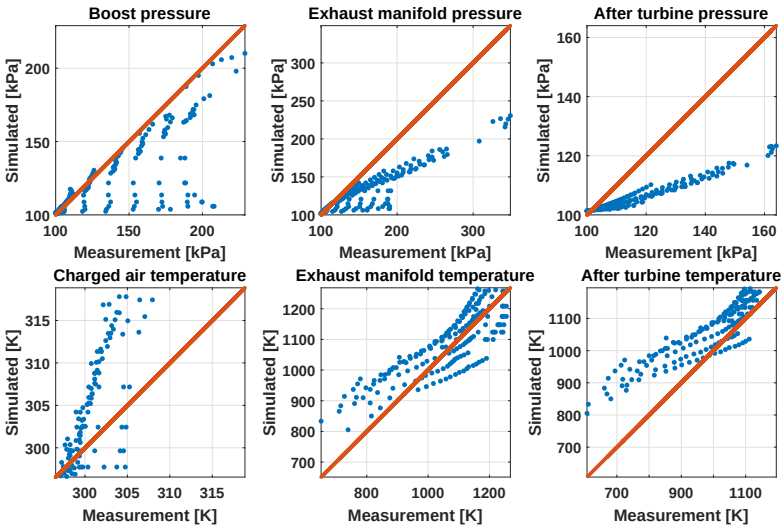

Figure 5.12: *The original simulation model is validated with test-bench that maintains correct mass flow and turbo speed. The results show signs of insufficient model quality both in the intake and exhaust side of the engine model.*

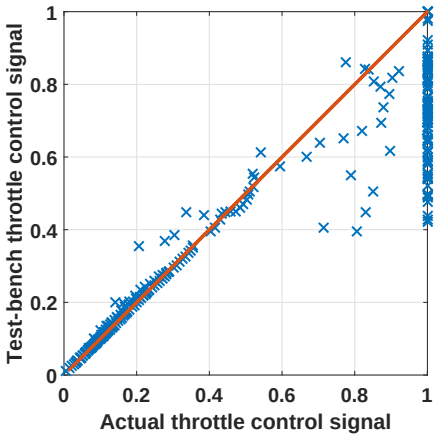

Figure 5.13: *The test-bench throttle control signal is compared with the actual throttle signal from the measurement data. The inconsistency can be seen and in many cases the test-bench needed to close the throttle more to be able to maintain correct mass flow.*

After substituting with the updated models, the comparison between simulation results and measurements is shown in Figure 5.14. The throttle test-bench signals are shown in Figure 5.15.

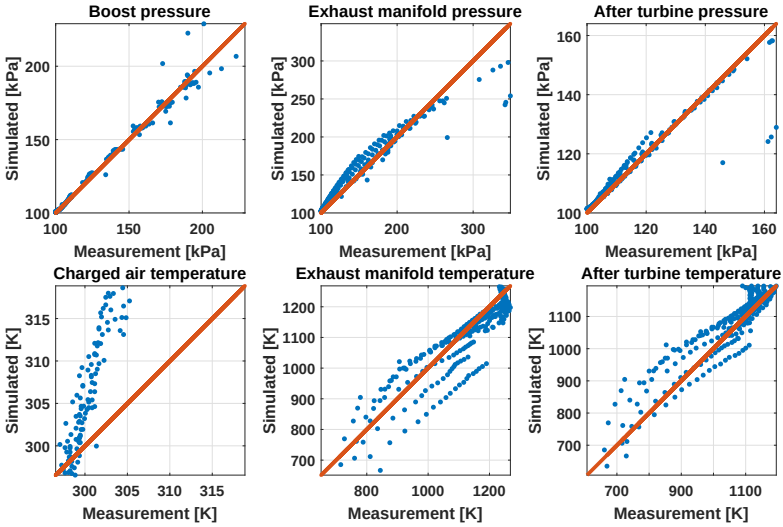

Figure 5.14: *The simulation model with updates done on the turbine and compressor is validated with test-bench that maintains correct mass flow and turbo speed. The improvement in simulated pressures is more significant than that in simulated temperatures.*

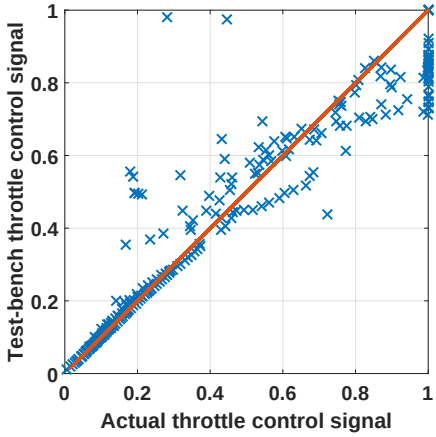

Figure 5.15: *The throttle test-bench signal is in greater compliance with the actual control signal.*

The updated model output without throttle test-bench is shown in Figure 5.16.

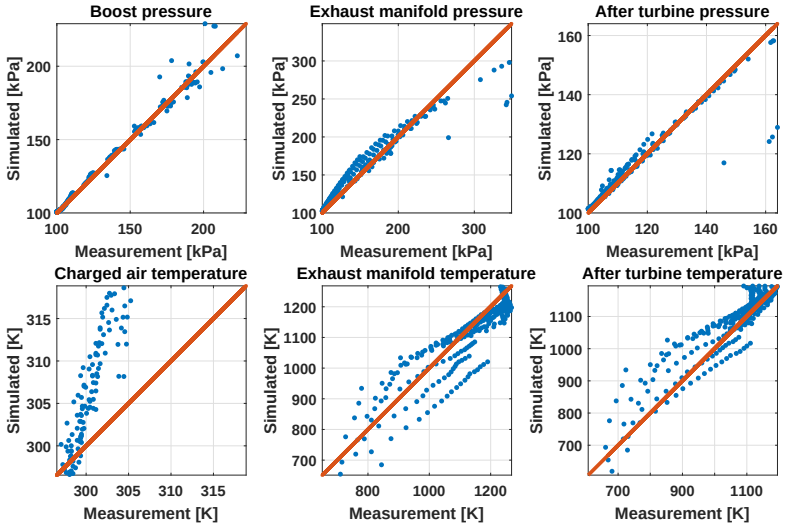

Figure 5.16: *The updated simulation model is validated with throttle test-bench disconnected. The improvement done is still visible.*

It is later discovered that the turbocharger installed in the engine test cell is different from the turbocharger from which the available measurement data was used to parametrise the simulation model. The dimension of the turbo charger in the engine test cell is smaller, and this resulted in different characteristics which can be seen in Section 5.13. Despite the fact that the turbocharger in the simulation environment and in the engine test cell have different properties, the control strategy for boost pressure shall remain universal and thus still suitable for model-based controller design.

5.5 Validation of Turbo Speed Set Point Calculation

In Section 4.2 the following three methods for calculating turbo speed set points are presented:

- Physical modeling.
- Look-up table generated by interpolation and extrapolation of compressor map.
- Curve Fitting of zero-slope.

The methods were tested on the data collected from the engine lab. During the data collection several steps were applied on the torque set point and the stock boost controller was used to generate the boost pressure. The tests were performed with different engine speeds and results are presented in Figures 5.18-5.20. A visualisation of the tests in the compressor map is shown in Figure 5.17.

In the estimations the intercooler effect were neglected, because of this the pressure after the compressor is assumed to be the boost pressure. The relative errors of the methods in relation to the boost pressure are also presented.

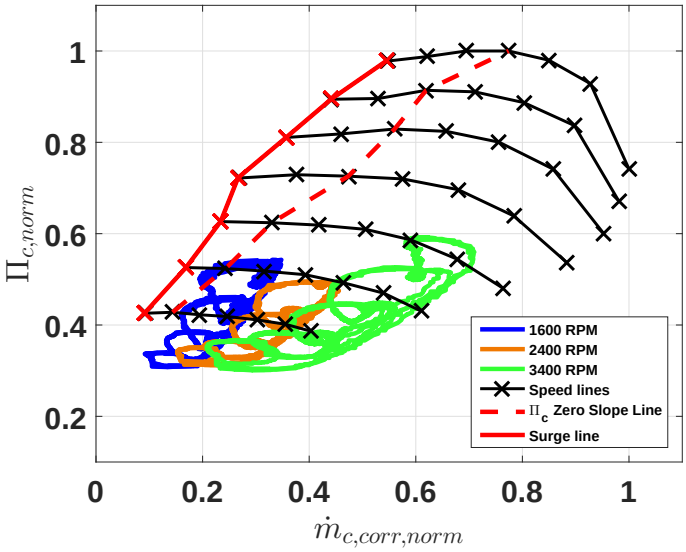

Figure 5.17: *The three different tests visualised in the compressor map. Intercooler effect were neglected and the boost pressures is used as the pressure after the compressor. It is seen that the test at 1600 RPM resides close to the zero-slope line and then for increasing engine speed the tests moves to the right, away from the zero-slope line.*

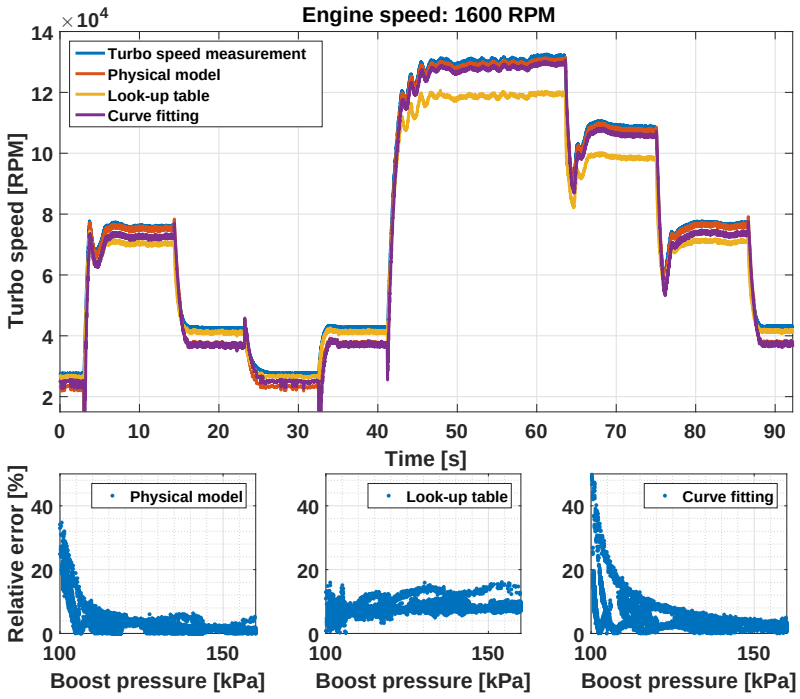

Figure 5.18: *Steps in requested torque at engine speed 1600 RPM were performed and the turbo speed is estimated with the three methods described in this thesis. In the upper plot the estimated speed and measured speed is presented. The relative error for the different models is presented in the lower plots. The look-up table seems to underestimate the turbo speed for higher turbo speeds. Apart from that all methods perform well at these test conditions.*

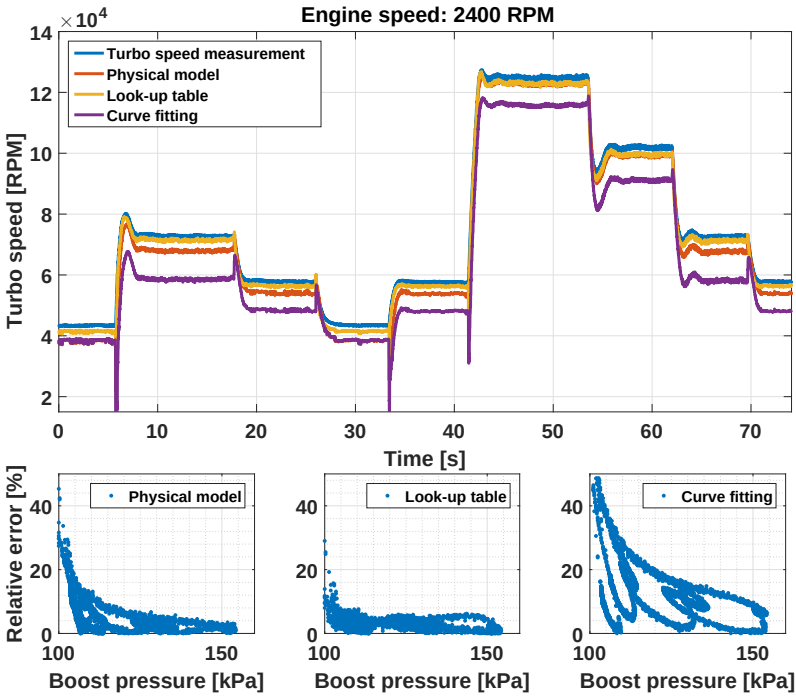

Figure 5.19: *Steps in requested torque at engine speed 2400 RPM were performed and the turbo speed is estimated with the 3 methods described in this thesis. In the upper plot the estimated speed and measured speed is presented. The relative error for the different models is presented in the lower plots. Look-up table seems to perform best and the zero-slope curve fit seems to underestimate the turbo speed.*

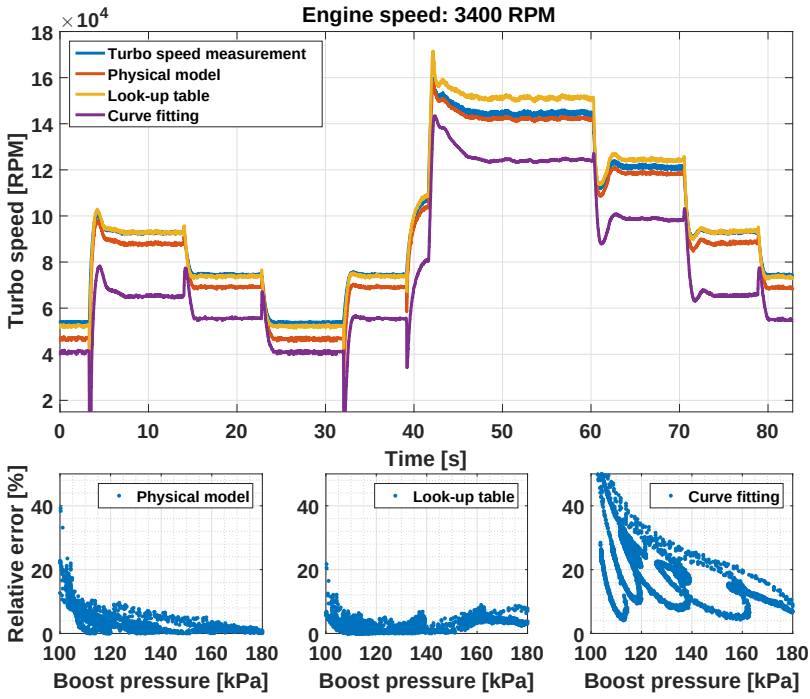

Figure 5.20: *Steps in requested torque at engine speed 3400 RPM were performed and the turbo speed is estimated with the 3 methods described in this thesis. In the upper plot the estimated speed and measured speed is presented. The relative error for the different models is presented in the lower plots. For this engine speed it is seen that the curve fit of the zero-slope underestimates the turbo speed.*

In the Figures 5.18 - 5.20 both the physical model and the look-up table do not change much between the test conditions. The zero-slope curve fit underestimate the turbo speed for the test cases with increasing engine speed. Also recall that in Figure 5.17 it was shown that higher the engine speed are in the tests further away the compressor drifts from the zero-slope.

5.6 Identification of Boost Pressure Dynamics

In Section 4.3 two different methods to estimate the time constants for the dynamic from turbo speed to boost pressure were presented. The following transfer

functions are used to present the result

$$G_{boost}(s) = \frac{K_{p1}}{1 + T_p s} \tag{5.1}$$

$$G_{speed}(s) = \frac{K_{p2}}{1 + T_t s} \tag{5.2}$$

$$G_{total}(s) = \frac{K_{p3}}{(1 + T_1 s)(1 + T_2 s)} \tag{5.3}$$

where $G_{boost}(s)$ is the system description used to evaluate when the turbo speed is used as input. $G_{speed}(s)$ and $G_{total}(s)$ is the system descriptions used for the identification of time constants. Different steps in the wastegate position with the electric wastegate actuator were perfomed and the turbo speed and boost pressure were measured. Engine speed and load were fixed during each engine speed. From this data, time constants for each step were calculated and for each engine speed the time constant were averaged. Test conditions and estimations are presented in Table 5.1, the averaged time constants is also visualised in Figure 5.21.

Table 5.1: *Estimated time constants and the test conditions are presented in this table. For each measurement all time constants for each measurement were averaged. Tot in the end of the table is the averaged time constants from each measurement. Load represents the air flow. Fit p % is the model fit when using turbo speed as input and Fit total % is the model fit when identifying the time constants.*

Data #	# steps	T_1 [s]	T_2 [s]	T_t [s]	T_p [s]	Fit p %	Fit total %	RPM	Load [g/rev]
1	5	0.41	0.13	0.48	0.05	92.3	91.2	1800	1.21
2	7	0.50	0.16	0.47	0.07	93.6	86.0	2000	1.22
3	10	0.34	0.09	0.33	0.09	96.6	93.1	2400	1.10
4	10	0.33	0.05	0.32	0.08	97.1	88.2	2800	0.96
5	10	0.30	0.11	0.31	0.09	97.1	89.6	3000	0.97
6	8	0.31	0.06	0.32	0.09	97.2	97.8	3300	0.84
7	8	0.34	0.08	0.35	0.08	96.2	93.2	3500	0.71
8	10	0.34	0.13	0.35	0.08	96.6	86.3	3600	0.71
9	9	0.33	0.09	0.36	0.08	96.2	93.7	4000	0.66
10	8	0.29	0.12	0.35	0.10	96.2	86.7	4200	0.64
11	10	0.31	0.10	0.33	0.09	96.1	93.0	4300	0.66
Tot	-	0.35	0.10	0.36	0.08	-	-	-	-

As seen in Table 5.1 identification using turbo speed is the most reliable method when comparing model fit but both methods estimate a time constant near each other. Using turbo speed as input the time constant, T_p, is 0.08 s. Comparing the time constant from wastegate position to turbo speed both models estimate a time constant near each other.

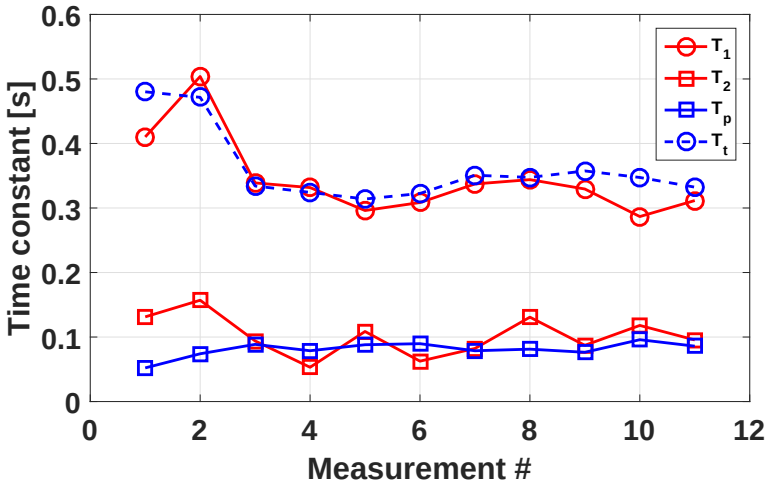

Figure 5.21: *Visualisation of the table content in Table 5.1, it is seen that the time constant from a wastegate position to turbo speed lies around 0.35 s and the time constant from turbo speed to boost pressure is around 0.10 s.*

5.7 Empirical Nonlinear Compensator

In Section 4.4.2 the design of the nonlinear compensator's development procedure used data from a different engine with a different turbocharger. The same procedures were repeated on the engine used during the thesis work to test the viability of the procedure. The results are presented in this section.

The measurement data and interpolation of measurement data with respect to air mass flow is shown in Figure 5.22. It can be seen that the turbo speed increases monotonically for each unique interpolated mass flow with the closing of wastegate. This observation is in agreement with the procedure done in Section 4.4.2.

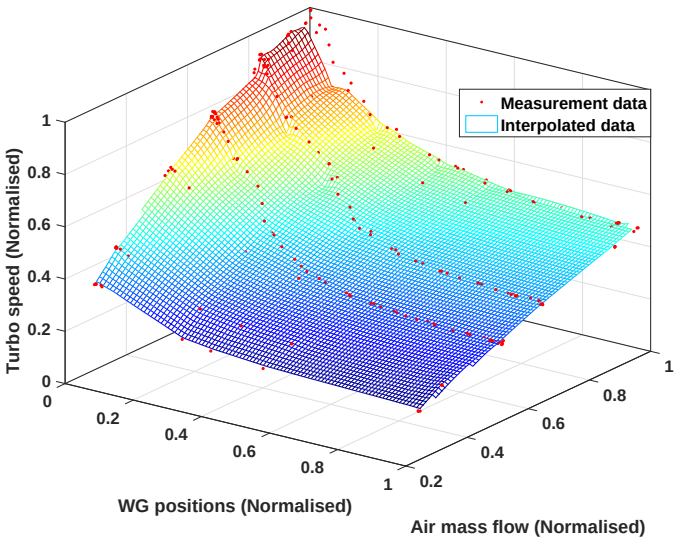

Figure 5.22: *Measurement data and interpolated measurement data for the empirical nonlinear compensator. The measurements were performed during the thesis work. Along with the closing of the wastegate the turbine speed increases monotonically for each unique interpolated mass flow.*

Recall the proposed nonlinear compensator function

$$N_t = a(\dot{m}_a)e^{-b(\dot{m}_a)u_{wg}} + c(\dot{m}_a) \tag{5.4}$$

and its final version

$$N_t = (a_1\dot{m}_a + a_2)e^{-bu_{wg}} + c_1\dot{m}_a + c_2 \tag{5.5}$$

It is now possible to validate if the proposal is in compliance with the measurement data collected during the thesis work. The estimated $a(\dot{m}_a)$, $b(\dot{m}_a)$ and $c(\dot{m}_a)$ is shown in Figure 5.23.

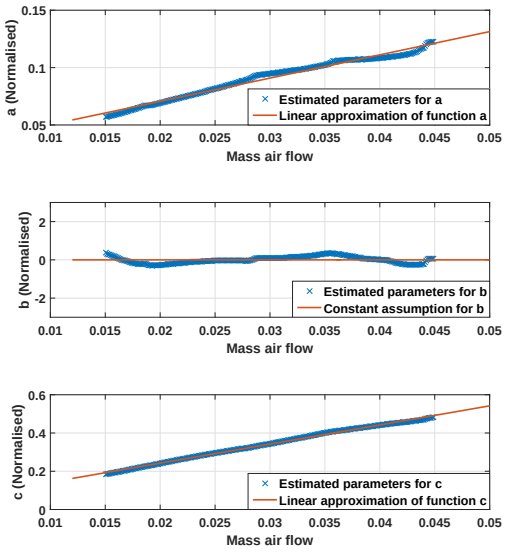

Figure 5.23: *The estimated a, b, and c as functions of mass air flow show that the same assumption as in* (5.5) *remains. (The a, b, and c parameters in the figure have been normalised and off-setted)*

a and c can be seen as linear functions of mass air flow whilst b remains constant. The parameters in (5.5) are identified accordingly. This is the same conclusion as in Section 4.4.2. When the inversion of the empirical nonlinear compensator function is used to calculate a wastegate position that resembles a turbo speed, Figure 5.24 shows how the calculated wastegate positions fits the measured positions and Figure 5.25 shows the calculation errors.

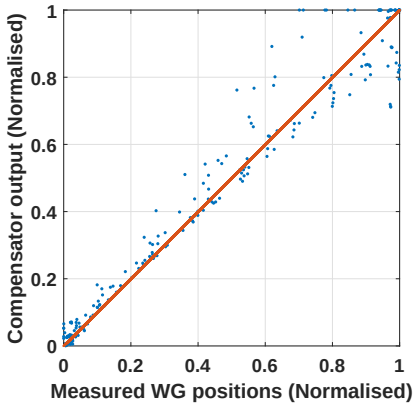

Figure 5.24: *The output of the inverted empirical nonlinear compensator function compared with the measured wastegate positions. The data are collected during the thesis work.*

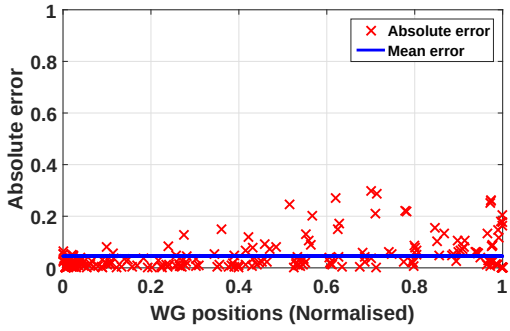

Figure 5.25: *Model errors in the empirical compensator function estimated by data collected during the thesis work. The errors are presented in absolute as calculations as relative errors would result in division by zero. The mean error lies around 0.046.*

5.8 Identification of Turbo Speed Dynamic System Model

Model estimation of turbine dynamic model was done by system identification from compensator converted wastegate valve position to turbo speed. An example of this conversion is visualised in Figure 5.26.

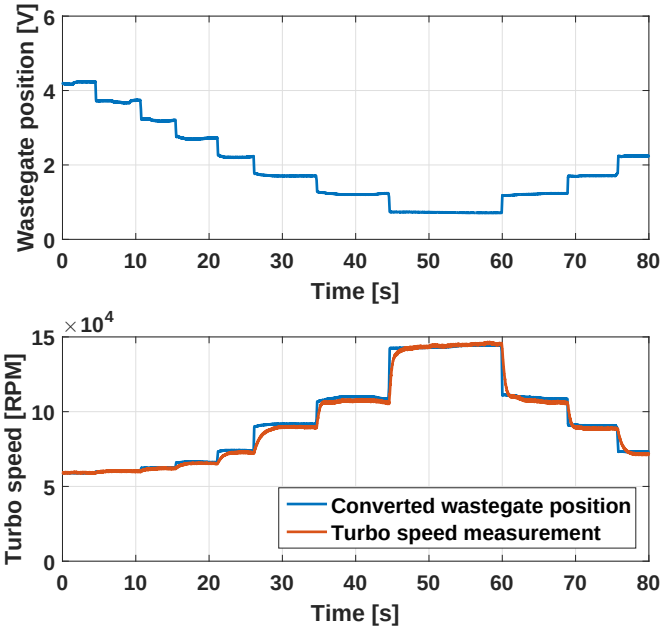

Figure 5.26: *The wastegate position measurement is shown in the upper figure. By using the nonlinear compensator function the positions is converted to virtual turbo speed signals which can be used for identifying the dynamic properties of the turbine. The converted wastegate position and the corresponding turbo speed can be seen in the lower figure.*

The result for system identification and fitness of the model is presented in Figure 5.27, the principle of cross-validation was used.

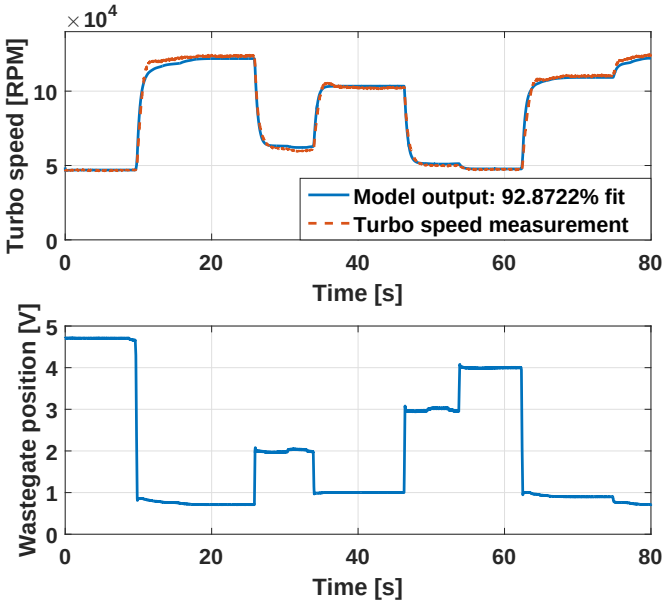

Figure 5.27: *The cross-validation is performed and shown in the upper figure. The in-signal for validation is wastegate positions and is plotted in the lower figure. The wastegte position was translated statically by the compensator function and was fed into the dynamic model. The model fits the measurement data by 92.87 %.*

The model identifications are performed for different engine operating points and the identified time constant, delay, and model fit are presented in Figure 5.28.

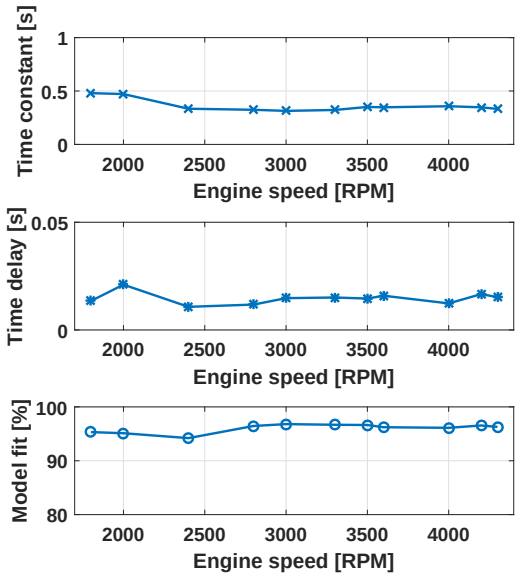

Figure 5.28: *The identified parameters for turbo speed dynamics from measurement performed in different engine speeds. The model fit for each identification is also shown.*

5.9 Model Identification of Actuator Motor

The identified model for electric actuator motor is tested with cross-validation. The validation data contains measurements where a combination of square pulses were used as input signal, and the result can be seen in Figure 5.29.

The estimated model fits the measurement data by 91.71 % according to normalised root-mean-square deviation method.

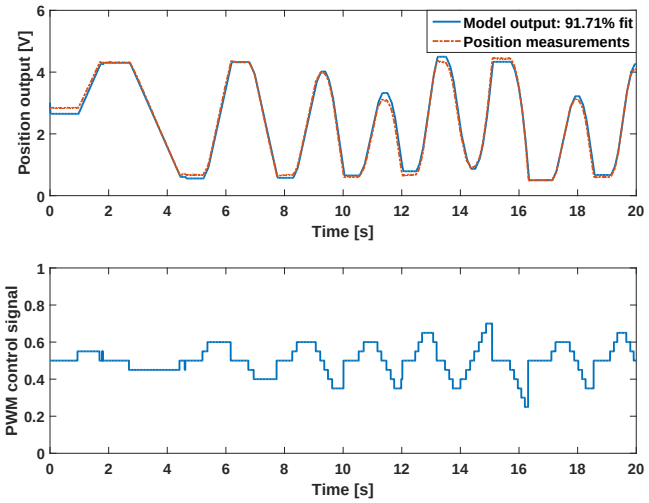

Figure 5.29: *Model validation of the wastegate actuator motor. The model fits the position measurements by 91.71 %.*

5.10 Electric Wastegate Actuator Controller

Results and behaviours from the implemented electric actuator controller and all complementary features are presented in this section. In Figure 5.30 the initialisation phase of the controller is shown. The controller performed a search pattern for the upper end position followed by the lower end position. After both end positions had been found and remembered, the position actuation proceeded to function normally.

The controller's response after a step in position set point is tested in both simulation environment and on the actuator unit. The result is shown in Figure 5.31.

The functioning soft landing and sealing features is demostrated in Figure 5.32. When soft landing is required, the PWM signal is tightened automatically. When the closing position is reached, the controller sends additional strength to the actuator shaft by applying extra PWM signal.

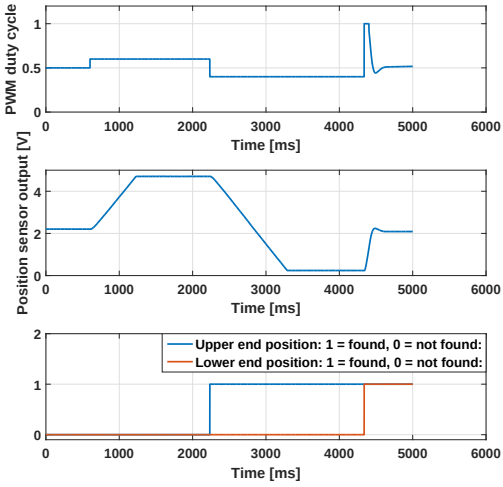

Figure 5.30: *The initialisation phase is performed. The controller attempted to find the upper and lower end positions respectively. The upper end position was found shortly after 2 seconds and after 4 seconds both positions was found and stored. Afterwards the controller began to maintain the demanded position set point.*

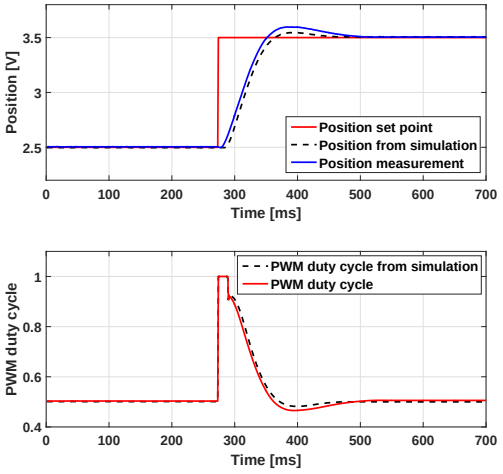

Figure 5.31: *Step response on actuator position. Both result from measurement from the actuator unit and result from simulation are presented and compared.*

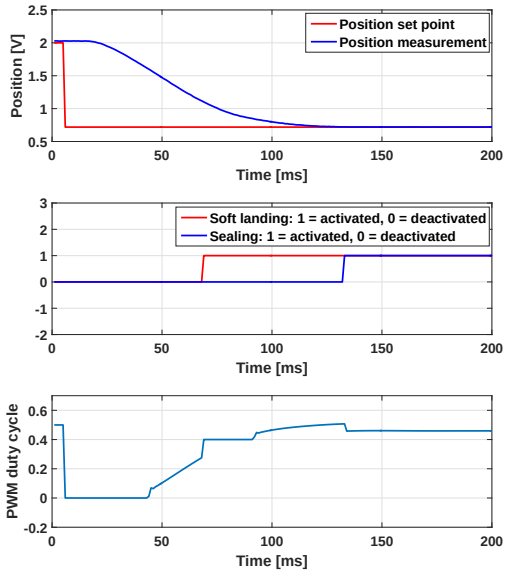

Figure 5.32: *The demonstration of soft landing and sealing features. The PWM signal is by default limited within 0 and 1 with 0.5 that corresponds to idle. In this demonstration when soft landing is activated, this limit is further tightened to* ± 0.1 *around 0.5, resulting the signal to be saturated immediately to 0.4 at* $t = 68$ *ms. When the set point is reached and the set point coincides with the closing position of the wastegate, the sealing function is activated. In this demonstration, a reinforcement by extra 0.05 of PWM is given.*

5.11 Observed Characteristics in Vacuum Actuated Wastegate

One observation that has been made on the vacuum actuator is the existence of saturation areas that occur near end positions of the travel. Within the saturation areas, changes in duty cycle could not cause movement of the shaft. The size of the saturation area are inconsistent and shifts depending on the engine operating points. This also leads to the phenomenon of hysteresis that exists during the movement of the vacuum actuator shaft. The non-linearities in the vacuum actuator is shown in Figure 5.33.

Another observation that has been made is the inconsistency of position actuation by a constant duty cycle on the vacuum actuator. This can be visualised in Figure 5.34. It can be seen that given a constant duty cycle input, different engine operating points could cause different displacements on the position actuations.

Since the electric actuator has feedback control and vacuum wastegate is con-

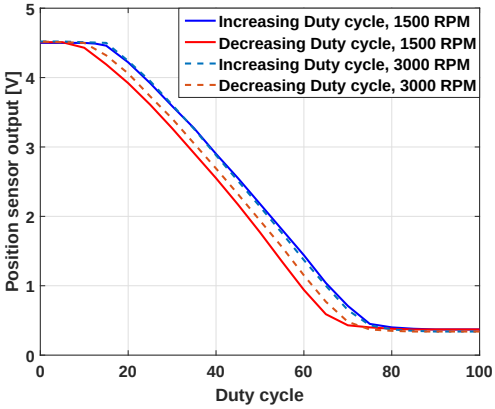

Figure 5.33: *The vacuum actuator is controlled by duty cycle input with no position feedback. The non-linearities that are visible are saturation and hysteresis. The differences in position and saturation areas during up-travel and down-travel are inconsistent for different engine operating points.*

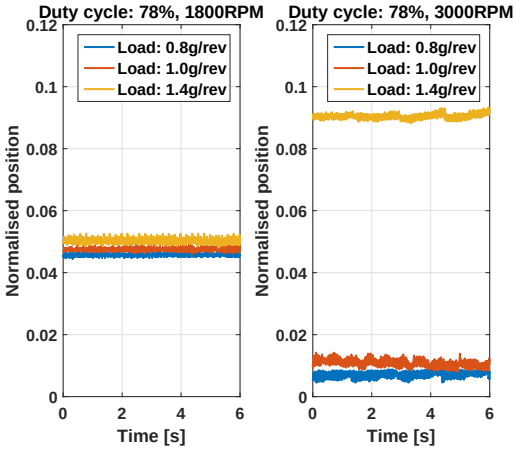

Figure 5.34: *A constant duty cycle of 78 % was applied on the vacuum actuator. The position output from the actuator is measured during different engine speeds and loads. It can be seen that during the measurement where engine speed was 1800 RPM the positions varied with different loads. When the engine speed was instead 3000 RPM the displacements became greater. The positions in the figures had been normalised: 0 stands for completely closed wastegate and 1 stands for fully open wastegate.*

trolled openly, the comparison of actuation speed is done by observing the time cost for both actuators to completely close from fully open position, as well as the other way around. The test was performed during different engine speeds

and the result is shown in Figure 5.35 and Figure 5.36.

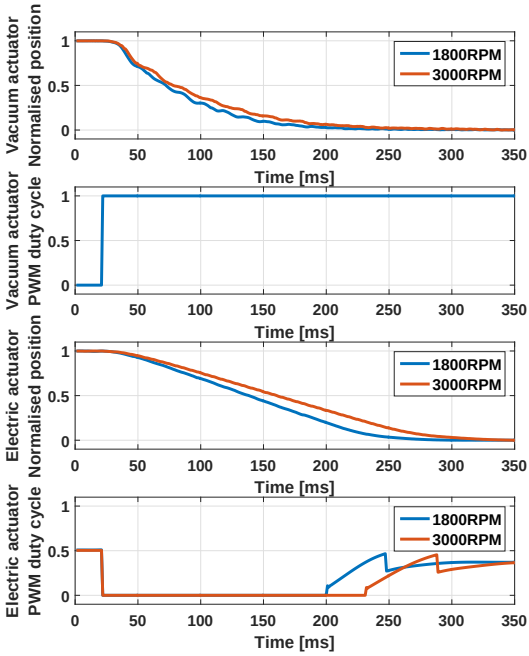

Figure 5.35: *From fully open to fully closed: the actuation speed of both actuators is tested at 2 different engine speeds. The control signals for the actuators is also shown. The positions in the figures had been normalised: 0 stands for completely closed wastegate and 1 stands for fully open wastegate. The activation of electric actuator's tightening function is also visible in the electric actuator PWM duty cycle.*

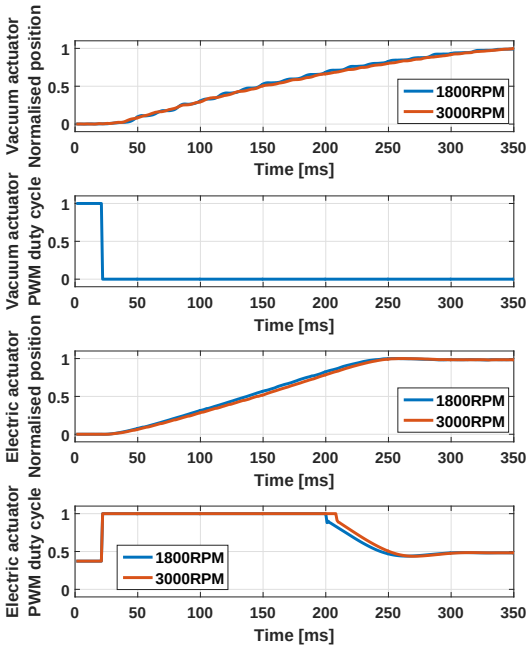

Figure 5.36: *From fully closed to fully open: the actuation speed of both actuators is tested at 2 different engine speeds. The control signals for the actuators is also shown. The positions in the figures had been normalised: 0 stands for completely closed wastegate and 1 stands for fully open wastegate.*

5.12 Pulsation Effects on Wastegate Valve

To observe the pulsations effect on the wastegate valve, the vacuum actuated wastegate were given a constant duty cycle of 75 %, which means that the wastegate valve were neither closed or fully open and had room to oscillate. The measurements were done at a constant engine speed and load.

Measurements of the pulsations with the electric actuated wastegate were done during steps in the demanded wastegate position because of the feedback control of the position it could not be measured the same way as for the vacuum wastegate actuator. The steps were performed during constant engine speed and load. The same input in position were used for all measurements and the input signal can be seen in Figure 5.39. DFT for the control signal during one of the measurements is shown in Figure 5.40, as can be seen no specific frequency is introduced from the position controller.

The wastegate position were sampled at 1000 Hz with an anti-aliasing filter and the DFT were computed to get the frequencies existing in the position measurements.

In Figure 5.37 and Figure 5.38 the different DFT for the position measurements are shown both for the vacuum wastegate and electric wastegate. The frequencies corresponding to the exhaust valves are also marked as vertical lines where RPS/2 is the frequency for each valve, RPS is the frequency for the engine and $2 \times$ RPS represent how often an exhaust valve opens. These frequencies is for a 4-stroke engine with 4 cylinders that ignite each cylinder at different times.

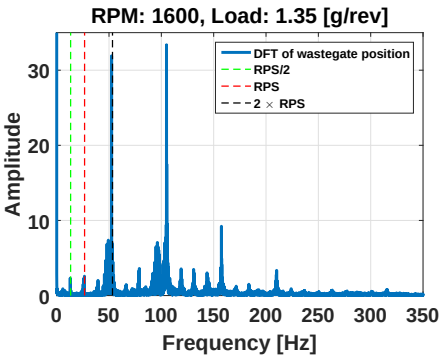
RPM: 1600, Load: 1.35 [g/rev]
DFT of wastegate position
RPS/2
RPS
2 × RPS
Amplitude
Frequency [Hz]

(a)

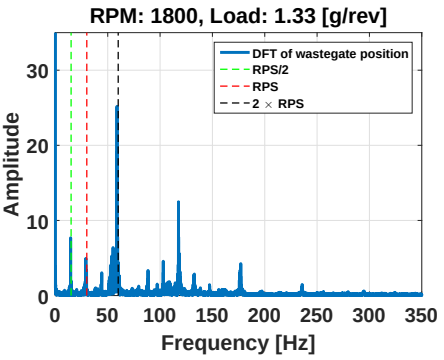
RPM: 1800, Load: 1.33 [g/rev]
DFT of wastegate position
RPS/2
RPS
2 × RPS
Amplitude
Frequency [Hz]

(b)

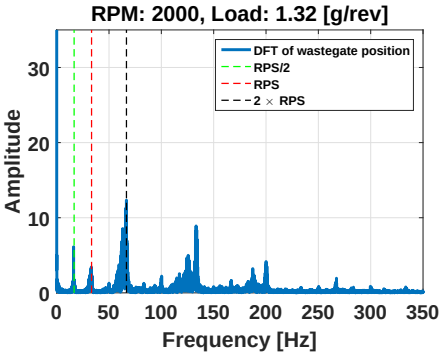
RPM: 2000, Load: 1.32 [g/rev]
DFT of wastegate position
RPS/2
RPS
2 × RPS
Amplitude
Frequency [Hz]

(c)

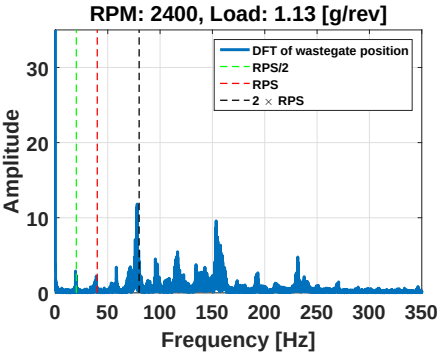
RPM: 2400, Load: 1.13 [g/rev]
DFT of wastegate position
RPS/2
RPS
2 × RPS
Amplitude
Frequency [Hz]

(d)

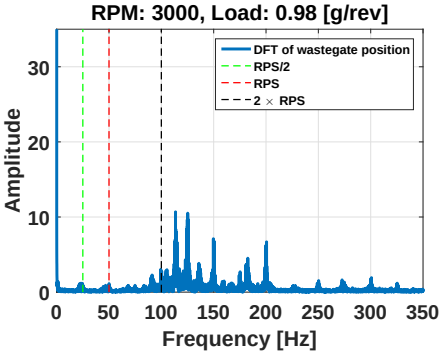
RPM: 3000, Load: 0.98 [g/rev]
DFT of wastegate position
RPS/2
RPS
2 × RPS
Amplitude
Frequency [Hz]

(e)

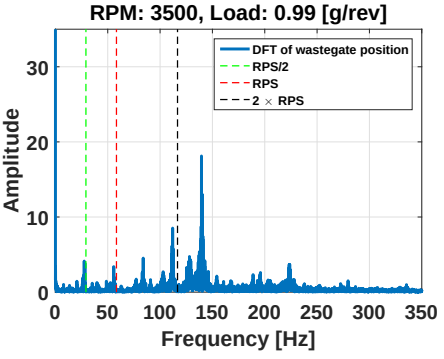
RPM: 3500, Load: 0.99 [g/rev]
DFT of wastegate position
RPS/2
RPS
2 × RPS
Amplitude
Frequency [Hz]

(f)

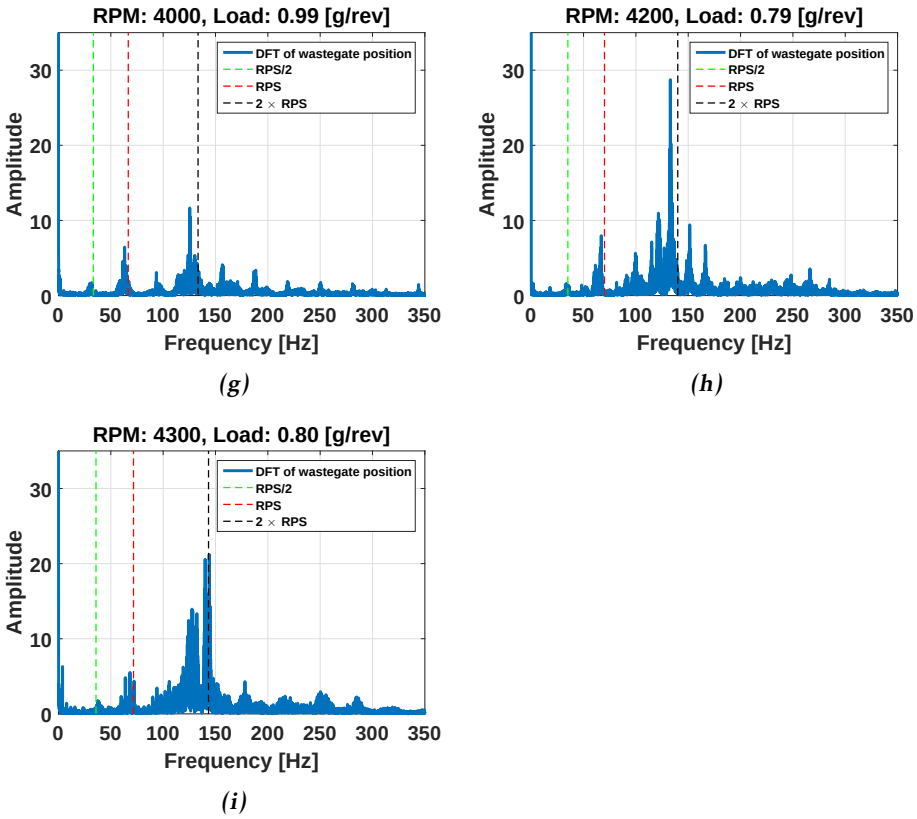

Figure 5.37: *DFT for the actuator controlled with vacuum. (a)-(i) are different speeds. The engine load is presented as the amount of air mass per revolution. Green dashed line is the frequency for when a certain cylinder opens its exhaust valve, red dashed line is the frequency that corresponds to engine speed, and the black dashed line is the frequency for when any exhaust valve opens. Frequencies connected to the engine speed and exhaust valves can be seen in all figures and multiples of these. For lower engine speeds the largest peak is for the peak corresponding with an exhaust valve opening. For higher engine speeds see for example (e) and (f) a peak at around 150 Hz is detected that is not explained by the frequency of the exhaust valves. When the frequency of the exhaust valve matches around 150 Hz this peak becomes larger and the surrounding frequencies also grow.*

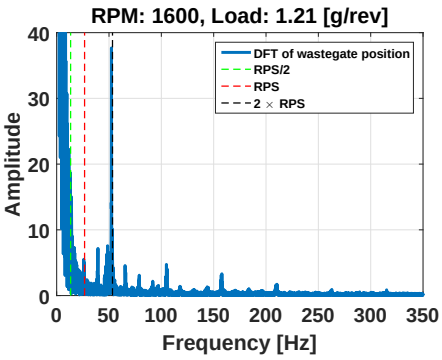
RPM: 1600, Load: 1.21 [g/rev]
DFT of wastegate position
RPS/2
RPS
2 × RPS
Amplitude
Frequency [Hz]

(a)

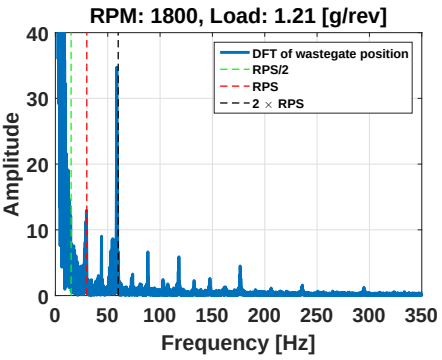
RPM: 1800, Load: 1.21 [g/rev]
DFT of wastegate position
RPS/2
RPS
2 × RPS
Amplitude
Frequency [Hz]

(b)

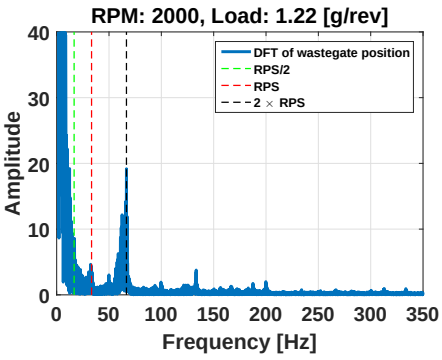
RPM: 2000, Load: 1.22 [g/rev]
DFT of wastegate position
RPS/2
RPS
2 × RPS
Amplitude
Frequency [Hz]

(c)

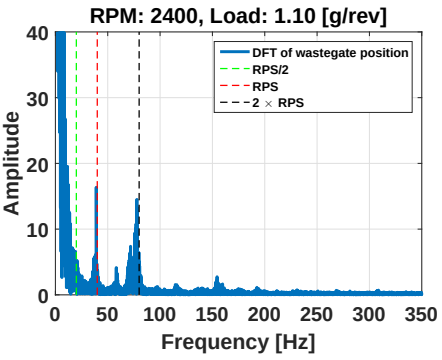
RPM: 2400, Load: 1.10 [g/rev]
DFT of wastegate position
RPS/2
RPS
2 × RPS
Amplitude
Frequency [Hz]

(d)

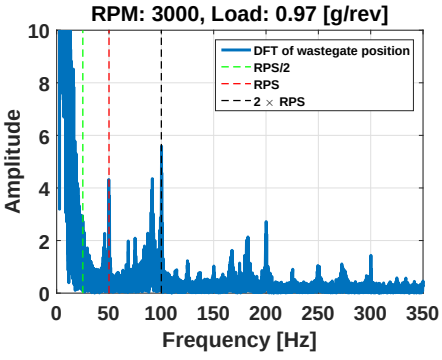
RPM: 3000, Load: 0.97 [g/rev]
DFT of wastegate position
RPS/2
RPS
2 × RPS
Amplitude
Frequency [Hz]

(e)

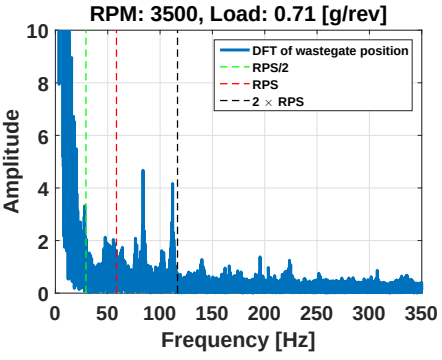
RPM: 3500, Load: 0.71 [g/rev]
DFT of wastegate position
RPS/2
RPS
2 × RPS
Amplitude
Frequency [Hz]

(f)

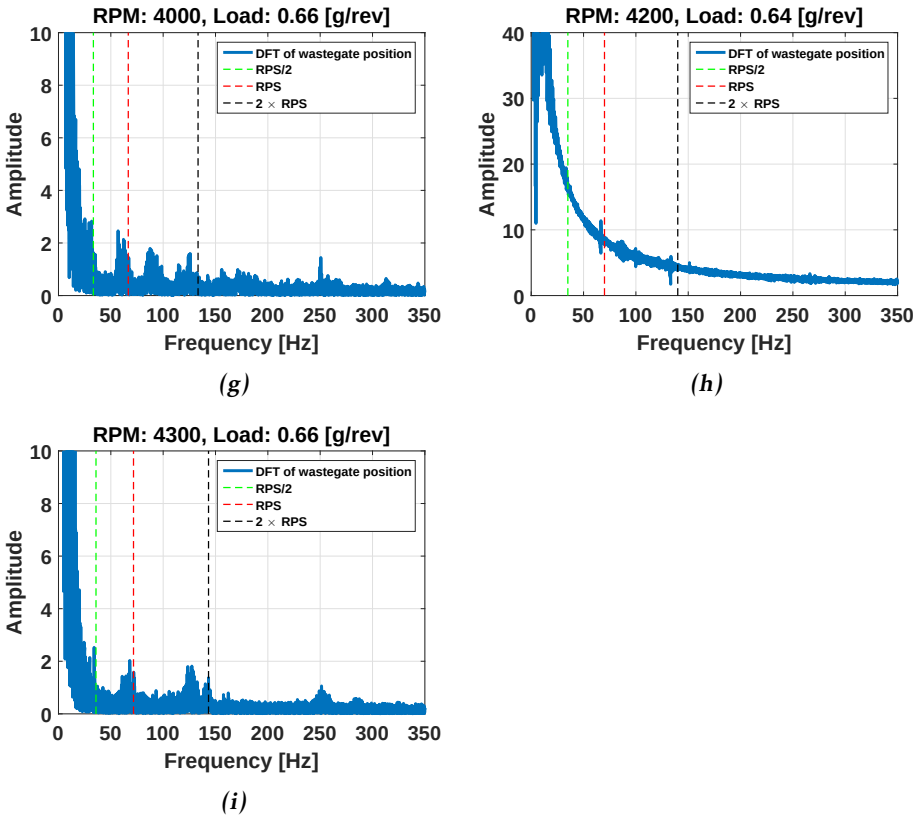

Figure 5.38: *DFT for the electric wastegate. (a)-(i) are different engine speeds and the engine load is presented as the amount of air mass per revolution. Green dashed line is the frequency for when a certain cylinder open its exhaust valve, red dashed line is the engine speed frequency, and the black dashed line is the frequency for when any exhaust valve opens. Frequencies connected to the engine speed and exhaust valves can be seen in all figures. The larger peaks that are visible to the right of the black dashed line for the vacuum controlled wastegate no longer exist here.*

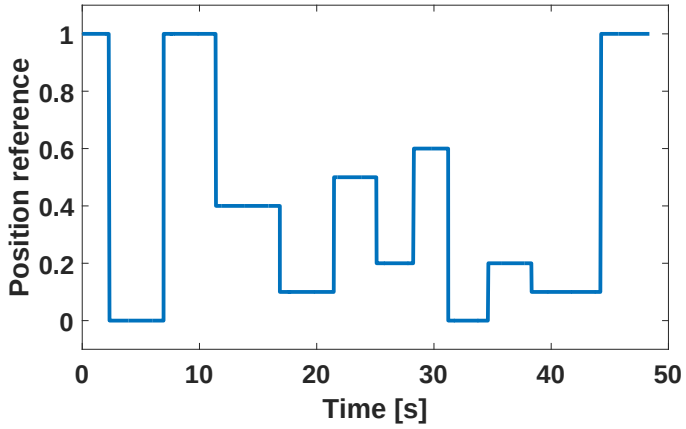

Figure 5.39: *Position reference for the electric wastegate during the steps. Same reference signal were used for all measurements.*

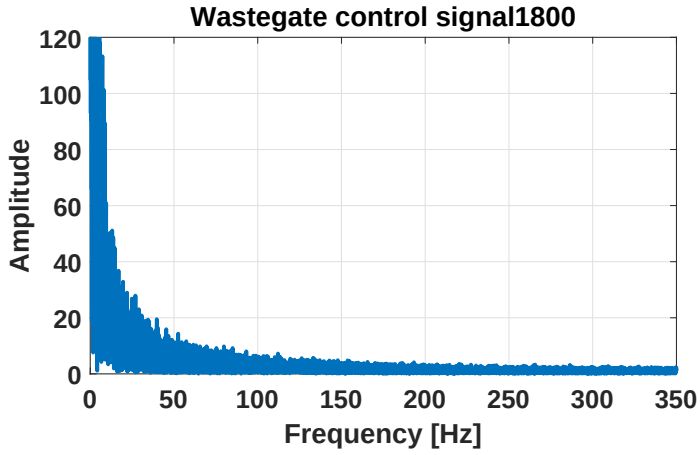

Figure 5.40: *DFT for the input signal to the electric motor. Showing that no specific extra frequency is introduced.*

As seen in Figures 5.37 and 5.38 the frequencies connected to the engine speed and exhaust valves is visible for all measurements. For the vacuum actuator a peak at around 150 Hz grows bigger with increasing engine speed and when the exhaust valve frequencies reaches around 150 Hz the peak becomes larger and the surround frequencies also grow. For the electric wastegate the dominating peaks are connected to the exhaust valve. Higher frequencies seem to be damped for the electric servo.

5.13 Controller Performance with Turbo Speed Sensor and Electric Wastegate

Initial design of the boost controller were done in the simulation environment. Later on these designs were tested and evaluated in an engine test cell. Unfortunately the simulation environment had a bigger turbo implemented than the engine in the test cell. The test of the boost controller were performed by holding a constant air mass flow through the engine by controlling the throttle and then make a step in boost pressure reference. The load is presented as air mass per revolution. For all tests in this section the load were set to 1.59 g/rev. This means that the air mass flow is increased for increasing engine speed and therefore the operating point moves further away from the zero-slope line in the compressor map with increasing engine speed. To calculate the turbo speed set point the zero-slope curve fit method described in Section 4.2 were used.

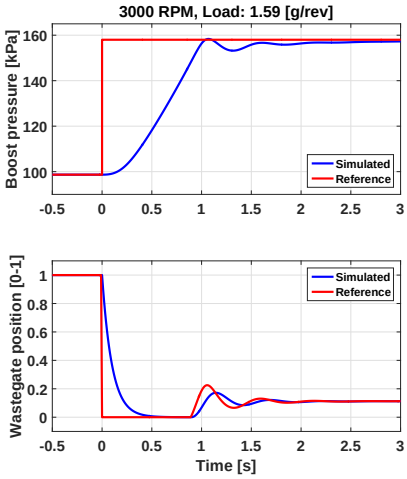

Figure 5.41: *Simulation of a step in boost pressure at 3000 RPM. It is seen that the wastegate is demanded closed directly when the step occurs. To reach the reference boost pressure first time takes approximately 1 second.*

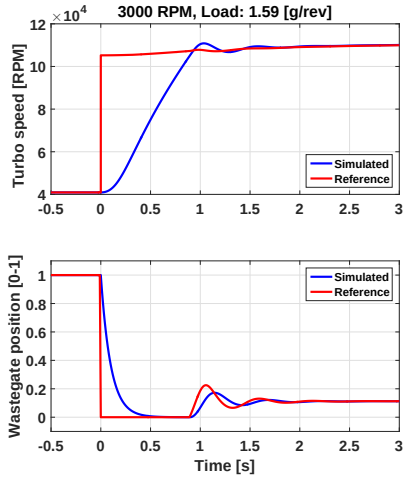

Figure 5.42: *Simulated turbo speed control during a step in boost pressure at 3000 RPM. As soon as the step occurs the feed forward can be seen as the initial step in the reference. This reference is then changed by the outer loop and also changes with the pressure and temperature before the compressor.*

In Figures 5.41 - 5.42 the simulation results of a step in boost pressure at 3000 RPM is presented. The wastegate position simulation is seen to have dynamics of a first order system. The turbo speed set point is fairly accurately estimated.

In Figures 5.43 - 5.44 a boost pressure step is performed at 3000 RPM. In

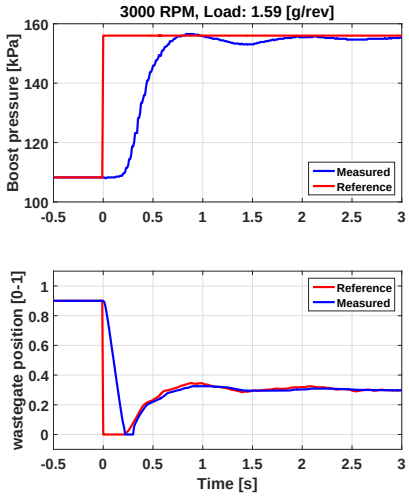

Figure 5.43: A step in boost pressure reference in an engine test cell at 3000 RPM. It is seen that the wastegate position is demanded closed directly and that it takes approximately 0.25 s for the wastegate to close. A delay of 0.25 s in boost pressure is also seen.

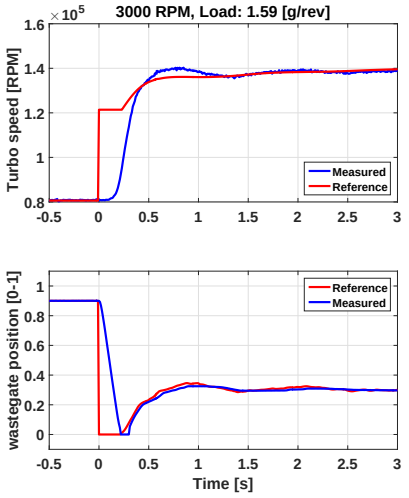

Figure 5.44: Turbo speed control during a step in boost pressure in engine test cell at 3000 RPM. Step in the turbo speed reference comes from feed forward, in this test the turbo speed is underestimated and a correction from almost 120 kRPM to 140 kRPM is seen.

this test it is seen that it takes approximately 0.25 s for the wastegate to close and a delay in boost pressure of about 0.25 s can also be seen. The turbo speed reference feed forward is also seen to be underestimated and a correction is done as soon as the wastegate position is not demanded closed.

In Figures 5.45 - 5.46 a boost pressure step is performed at 2000 RPM. The same sort of delay in boost pressure and the time to close the wastegate is seen as for 3000 RPM. Turbo speed reference is not needed to be corrected as much as in the case for 3000 RPM, the initial feed forward of turbo speed is almost enough.

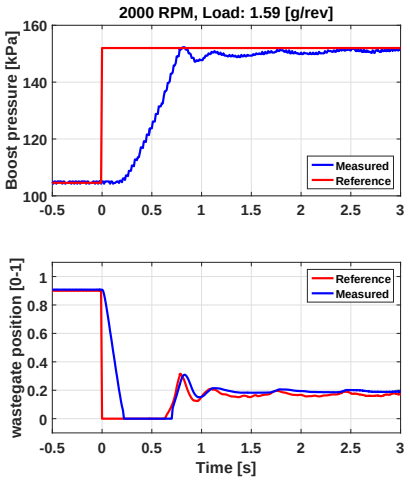

Figure 5.45: *A step in boost pressure reference in an engine test cell at 2000 RPM. It is seen that the wastegate position is demanded closed directly and that it takes approximately 0.25 s for the wastegate to close. A delay of 0.25 s in boost pressure is also seen.*

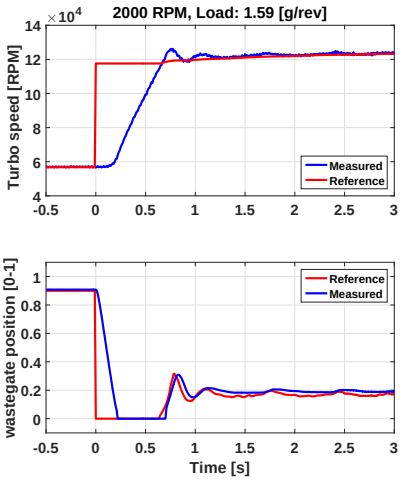

Figure 5.46: *Turbo speed control during a step in boost pressure in engine test cell at 2000 RPM. Step in the turbo speed reference comes from feed forward, in this test the turbo speed is almost correct and only a small correction of the reference is seen.*

6

Conclusions and Future Work

A new strategy for controlling boost pressure is presented. The way this strategy stands out is that the turbo speed is also used as a controller feedback signal together with boost pressure measurements. Furthermore the actuation of wastegate position is switched from vacuum actuator to an electric actuator.

Model-based design has been a central part of the thesis work, including both simulation environment and controller structure design. The existing engine MVEM model, developed by the staff at Linköping University, has been updated by new model structures for turbine and compressor in order to improve simulation. These new models are introduced in Chapter 3.

Different controller strategies and structures have been proposed and analysed. The control strategy which has been chosen to further perform boost control in the engine test cell utilised cascade controller structure. The cascade controller consists of an outer loop which controls the boost pressure by calculating the turbo speed set-point for the inner loop. The inner loop controls the turbo speed according to outer loop's demands. Both controllers include measurement feedback by which the outer loop uses boost pressure measurement and the inner loop uses turbo speed measurement. The electric actuator has also its own position feedback, and the controller design for the actuator is discussed in this thesis work as well.

During the thesis work questions came up concerning preferences of model structures, control structures, and choice of components and hardware. The conclusions that have been made after the thesis work are summarised in this chapter.

6.1 Comparison and Preference of Compressor Mass Flow Model and Efficiency Model

In Figure 5.1 the red speed lines are not as compact as wanted to be well fitted by the basic ellipse model. Distance between speed line and model will have a direct effect on the error. It is seen for example that the basic ellipse model for $\Psi_{norm} = 0.8$ underestimates Φ_{norm} for all speed lines except one that has 2 solutions. This underestimation would result in an underestimation of the compressor mass flow, $\dot{m}_c$.

Benefits with the basic ellipse model are that it only have 2 parameters to determine and a low computational cost in simulations. As shown in Figure 5.2 the basic ellipse model has a mean relative error of 17.75 % which could be seen as a bias error. This bias is because of the effects seen in Figure 5.1 where it is a distance between the speed lines and the ellipse model for almost all measurement points.

It is seen from Figure 5.2 and 5.3 that the extended ellipse model has bigger outliers than the basic ellipse model. When comparing the mean relative error of basic ellipse model and extended ellipse model it is seen that the extended ellipse model is more accurate than the basic ellipse model. Because of this the extended ellipse model has been used in the MVEM in this thesis.

As for the compressor efficiency model, a 2.14 % mean relative error can be seen in Figure 5.4. With a more advanced model this error could probably be decreased but it would also most likely increase the simulation time. For experiments conducted during this thesis work the accuracy seen in Figure 5.4 is considered enough.

6.2 Comparison and Preference of Turbine Mass Flow Model

For modelling the mass flow through a rotating turbine, a physical restriction model and a non-physical square root model are introduced. The model errors are presented in Figure 5.5 and 5.6. The physical restriction model has marginally smaller errors when measured with mean error, the model also requires knowledge of two variables to be able to calculate the third. This drawback is however negligible in the case where the turbine speed is measured directly. On the other hand the non-physical square root model is appreciated when the information of turbine speed is kept unknown. Despite the simplicity of the non-physical square root model the mean error and relative errors lies under 3.2 %. The uncomplicated nature of this model may benefit both speedy simulations and fast on-line calculations when embedded in a controller algorithm. When the speed dependency is neglected, the inversion of the equation becomes trivial as the model describes a direct relationship between mass flow and pressure ratio.

6.3 Comparison and Preference of Turbine Efficiency Model

The quality of the BSR model is poorer within the lower pressure ratio range ($\Pi_t < 2.5$) which is the normal operation range of the turbine on the production engine. The uncertainties go as high as 9.2 % which may jeopardize the estimation of turbine torque output along with the after-turbine conditions.

The model errors in the new turbine efficiency model are lower and appears more uniform when compared with the BSR approach. When applied to a simulation environment or control strategy the a and b parameters in this model can be parsed by using look-up table with suitable interpolation and extrapolation methods in order to adapt to hardware limitations in calculation load.

6.4 The Engine Simulation Environment

An engine simulation model is used to gain productivity on the boost controller design throughout the whole thesis work. The engine simulation model has been updated from the original model that had been made available in the beginning of the thesis work.

In Section 5.4 the improvement on the turbine and compressor models is shown. The simulation of boost pressure as well as pressures in exhaust manifold and after turbine have been greatly improved. However the modelling of temperatures gained only marginal enhancement.

The engine simulation model was used extensively for designing and testing the principles of control strategies prior implementation in the engine test cell. As also shown in Section 5.13 the engine simulation model was able to provide fundamental insight on how the controller ought to behave on the real engine, despite the fact that a different turbocharger was installed in the engine test cell.

6.5 Identification of Turbo Speed Dynamics

The dynamic behaviour of the wastegate-controlled turbo speed is assumed to have nonlinear gain and linear dynamics. The identification was performed according to the work flow: first convert wastegate position with compensator function, then perform identification of time constant and time delay. From the results collected in the engine lab, this work flow worked as expected and the identified turbine dynamic model fits the measurement data well.

The identification was also performed during different engine speeds, and through Figure 5.28 the identified time constants and time delay showed little deviations while fitness of the identified models remained high. This also conclude the reasonableness of the assumption suggested in Section 4.4.

6.6 Electric Wastegate Actuator

For designing a control strategy for the electric actuator, a system model was estimated. The estimated model fits the validation data with 91.71 % correctness which is considered sufficient for the continuation of the controller design.

The initialisation sequence for the electric actuator functions as expected. The upper and lower end positions can be successfully detected and memorised by the controller. The complementary functions for soft landing and sealing also worked as designed. In order to visualise the principle of work for the soft landing function, the threshold for activation of the function was increased so the saturation of PWM control signal can be seen in Figure 5.32. In practice, this can lead to unnecessary over-cautiousness and may slow down the actuation. The softlanding function is designed to serve solely as a safety precaution and should not affect the controller performance. In the final version of the controller the parameters in this function have been tuned so that it only activates when the position overshoot is harmfully large.

During the step-response test, the electric actuator reacted both responsively and accurately with an acceptable amount of overshoot over the set point. The calculated PWM control signal has no overreactions and noises. It had also come to knowledge after engine experiments that the state-feedback controller needs little to none compensation from the accompanying I-controller. The disturbance from the wastegate flow is insufficient to cause too much stationary errors for the state-feedback controller to handle. Furthermore it is worth to point out that the simulation model for both the actuator and the associated controller is in consistence with the measurements from the actual unit in the engine lab. This observation also confirms the practicality of the design procedure introduced in Section 4.5.

6.7 Comparison Between Electric and Vacuum Wastegate Actuator

In term of actuator speed for the specific components used during the thesis work, the comparison depends on whether the actuation is towards opening or closing of wastegate.

The actuation towards closing of wastegate is shown in Figure 5.35. In this demostration the vacuum actuated wastegate took less time to reach complete close than the electric actuator. However the vacuum actuator could not maintain a constant movement speed and it became slower as it approached the closing position. On the other hand, Figure 5.36 shows the travel from closed to open wastegate, and the electric actuator performed at least 100 milliseconds faster than the vacuum actuator.

The closing mechanism of vacuum actuator works by releasing the spring inside the actuator, and vacuum is used to compress the spring during the opening mechanism, causing differences in actuating speed. The electric actuator functions in the same manner no matter directions of motion. When a controller in-

teracts with the electric actuator it should expect consistent behaviour, however if the vacuum actuator is instead used case-separation may be required depending on the direction of actuator movement.

The amount of boost pressure is generated mainly by varying turbo speed, which is controlled directly by positioning the wastegte valve. The wastegate actuator's capability to accurately maintain a position is therefore important for the dependability of the boost controller. As described in Section 4.5 and Section 5.10 the motor in the electric actuator is a linear system that has consistent relationship between input and output. This is however not the case for the vacuum actuated wastegate as it suffers from problems such as hysteresis and positioning inconsistency in different operating conditions of the engine. The procedures to develop the model and controller for the vacuum actuated wastegate is discussed in Thomasson et al. (2013) and Thomasson et al. (2009). As the electric actuator is mostly linear except for the hardware limits in positions, to design a controller for a linear system is more straight-forward than that for a nonlinear one.

The problem of inconsistent position actuation by the vacuum actuator's duty cycle may impose requirement on the complexity of the boost controller. If the controller design uses a model-based approach, the controller has to gain additional knowledge about how the position behaves during different engine operating points. However if the position uncertainties can be eliminated by a feedback controller, such as an electric actuator, it may simplify the structure of the boost controller.

As analysed in Section 5.12, the position of vacuum actuator is not immune from exhaust gas pulsations and other disturbances. The position feedback of electric actuator is low-pass filtered to avoid explicitly counteracting exhaust gas pulsations, however the higher frequencies that affect positions of vacuum actuator seems unable to affect the electric actuator.

The conclusion being that the electric actuator is preferred when it comes to control of position. The position feedback together with consistent actuation speeds makes the wastegate flow model more trustworthy thus favours the model-based design of boost pressure control. The strength of the position holding can be easily made stronger than that of vacuum actuator. The force applied by the electric motor is adjustable which enables the user to adjust between disturbance suppression and noise sensitivity.

6.8 Boost Control with Turbo Speed Sensor

One of the objectives with this thesis was to establish a fair baseline measurement when comparing control strategies with and without the use of a turbo speed sensor. A fair comparison is almost impossible to make because that would require the development of two different controllers, one with the turbo speed and one without. Both controllers need also to be optimal to prevent biased result due to bad calibration of any one of them. The comparison is therefore unrealistic and it is more relevant to discuss what information the turbo speed would add when used.

In Section 5.6 it was shown that the time constant from turbo speed to boost pressure is approximately 0.08 second. Because of this the measurement of the turbo speed sensor compared to the boost pressure sensor would quicken the feedback by eliminating that time constant. Furthermore compared to boost pressure measurement the turbo speed measurement is less exposed to disturbances affected by the throttle.

Investigating results from boost pressure step-response presented in Section 5.13 a delay in boost pressure response was presented. The delay is believed to originate from the time it takes to close the wastegate. The wastegate maintains closed until the boost pressure almost reaches its set-point. The time cost to perform these actions are caused by the actuation performance and inertia of the turbine, hence is not subject to be improved by introducing turbo speed sensor. What the turbine speed sensor would improve is the opportunity to control what happens when the boost pressure set-point is almost reached. The faster feedback provided by the turbo speed measurement would ease prevention of overshoot and oscillations than if only the boost pressure sensor were to be used.

The most challenging part in boost pressure control is believed to be the adjustment after that the turbine has almost reached the desired speed. Investigating the measurements in Section 5.13 once again it can also be seen that the turbo speed and boost pressure are strongly connected. Oscillations in turbo speed are visible as similar oscillations in boost pressure.

In Section 5.11 it was shown that the vacuum actuator was faster in closing the wastegate than the electric actuator. This would indicate that the vacuum actuator would be able to decrease the rise time to reach desired boost pressure. However the opening mechanism performed by the vacuum actuator were slower and it was also shown to have hysteresis and a inconsistency in position depending on surrounding conditions. This leads to the argument that the electric actuator would be superior to prevent unwanted overshoots and oscillations in boost pressure. Electric actuator in combination with the faster feedback provided by turbo speed sensor would also give rise to faster actuation against overshoots and oscillations and make the controller more robust.

The controller structure for boost pressure presented in the thesis where one controller handles boost pressure and another handles the turbo speed may not be suitable for implementation. It was also shown that the dynamics from wastegate position to turbo speed were slower than the dynamics from turbo speed to boost pressure which is in conflict with one of the principles behind cascade control strategy, where the inner loop dynamics needs to be faster than the outer loop's.

Controlling the turbo speed solely may not be the best way to achieve optimal boost pressure generation except the turbo speed sensor could give a better insight of the mass flows at the engine inlet. This could open up possibilities for model based control strategies that combine several actuators and sensors.

6.9 Future Work

There are aspects that are believed to further refine the thesis work if sufficient time and lab resources were given. The aspects are listed below in hope to stimulate future developments of engine simulation and turbo control.

1. Investigate possibilities to improve temperature models in the simulation environment. Several updates have been performed on the turbine and compressor during the thesis work and the simulation quality of pressures has been greatly improved. While the modelling of temperatures have somewhat also gained improvement, it would be worth to investigate better models to further reduce errors.

2. Reduce actuator travel distance. It is seen in the steady state analysis of relationship between wastegate position and turbo speed that there is an area within the actuator travel that did not result significant changes in turbine speed. This area is around 30 % of the whole travel distance from the fully open position and is of lesser necessity for the turbo speed control. The actuation time can therefore be further reduced by shorten the actuation distance.

3. Alternative turbo speed controller structure.

    - The nonlinear compensator function that is introduced in the turbine speed controller is incapable to handle disturbances in the mass flow as only set-points of the mass flow were used as input. The compensator function can be made more accurate if the mass flow immediately after the exhaust valves can be modelled and used by the compensator.
    - The boost controller can gain awareness of the disturbances by using a model-based state-feedback controller with mass flows, temperatures, pressures, and turbo speed as states. By introducing turbo speed sensor states connected to the turbocharger can be more accurately estimated and therefore gives a better insight about the states.
    - As both throttle and wastegate can be used to regulate the mass flow and pressures through engine intake it may be advantageous to investigate possibilities of multi-variable controller. The controls of throttle and wastegate may be combined. The cooperation of throttle and wastegate controllers could also be optimised by using optimal control strategies.

4. In the thesis it is believed to be the position control of the wastegate that is of importance for the control of the turbine. To further compare a vacuum wastegate and an electric motor it is believed that both should be compared using position control. Because of what was presented in this thesis the vacuum wastegate has been shown to have non-linearity and inconsistency in control signal and position that could make it hard to implement an effective position control.

Bibliography

Per Andersson. *Air Charge Estimation in Turbocharged Spark Ignition Engines*. PhD thesis, Linköpings Universitet, 12 2005. Cited on pages 5, 7, 9, and 20.

Massimo Capobianco and Silvia Marelli. Waste-gate turbocharging control in automotive si engines: Effect on steady and unsteady turbine performance. In *SAE Technical Paper*. SAE International, 08 2007. doi: 10.4271/2007-01-3543. URL http://dx.doi.org/10.4271/2007-01-3543. Cited on page 4.

Nicolò Cavina, Davide Moro, Matteo De Cesare, and Gabriele Serra. Exhaust gas turbocharger speed measurement via acoustic emission analysis. In *SAE Technical Paper*. SAE International, 04 2008. doi: 10.4271/2008-01-1007. URL http://dx.doi.org/10.4271/2008-01-1007. Cited on page 3.

Rick Dehner, Neil Figurella, Ahmet Selamet, Philip Keller, Michael Becker, Kevin Tallio, Keith Miazgowicz, and Robert Wade. Instabilities at the low-flow range of a turbocharger compressor. *SAE Int. J. Engines*, 6:1356–1367, 05 2013. doi: 10.4271/2013-01-1886. URL http://dx.doi.org/10.4271/2013-01-1886. Cited on page 3.

Martin Enqvist, Torkel Glad, Svante Gunnarsson, Peter Lindskog, Lennart Ljung, Johan Löfberg, Tomas McKelvey, Anders Stenman, and Jan-Erik Strömberg. *Industriell Reglerteknik Kurskompendium, Course Material in Industrial Control Systems*. Bokakademin Linköping, 2014. Cited on pages 3, 24, 35, 37, 46, 47, and 48.

Lars Eriksson and Lars Nielsen. *Modeling and Control of Engines and Drivelines*. John Wiley & Sons, 2014. Cited on pages 3, 4, 7, 8, 14, 15, 16, 17, 18, 26, and 39.

Lars Eriksson, Vaheed Nezhadali, and Conny Andersson. Compressor flow extrapolation and library design for the modelica vehicle propulsion library - vehprolib. In *SAE 2016 World Congress & Exhibition*, number SAE Technical Paper 2016-01-1037, Detroit, United States, April 2016. Cited on pages 28, 29, and 33.

Torkel Glad and Lennart Ljung. *Reglerteknik, Grundläggande teori*. Studentlitteratur Lund, 2012. Cited on pages 20 and 49.

Torkel Glad and Lennart Ljung. *Reglerteori. Flervariabla och olinjära metoder*. Studentlitteratur Lund, 2014. Cited on pages 3 and 23.

Fredrik Gustafsson. *Statistical Sensor Fusion*. Studentlitteratur Lund, 2012. Cited on page 48.

Fredrik Gustafsson, Lennart Ljung, and Mille Millnert. *Signal Processing*. Studentlitteratur Lund, 2011. Cited on pages 49, 52, and 53.

Jamil El Hadef, Guillaume Colin, Yann Chamaillard, and Vincent Talon. Physical-based algorithms for interpolation and extrapolation of turbocharger data maps. *SAE Int. J. Engines*, 5:363–378, 04 2012. doi: 10.4271/2012-01-0434. URL http://dx.doi.org/10.4271/2012-01-0434. Cited on pages 4, 19, 58, and 60.

Elbert Hendricks. A compact, comprehensive model of large turbocharged, two-stroke diesel engines. In *SAE Technical Paper*. SAE International, 09 1986. doi: 10.4271/861190. URL http://dx.doi.org/10.4271/861190. Cited on page 4.

Elbert Hendricks and Spencer C. Sorenson. Si engine controls and mean value engine modelling. In *SAE Technical Paper*. SAE International, 02 1991. doi: 10.4271/910258. URL http://dx.doi.org/10.4271/910258. Cited on pages 4 and 9.

J.-P. Jensen, A.F. Kristensen, S.C. Sorenson, N. Houbak, and E. Hendricks. Mean value modeling of a small turbocharged diesel engine. In *SAE Technical Paper*. SAE International, 02 1991. doi: 10.4271/910070. URL http://dx.doi.org/10.4271/910070. Cited on page 4.

Amey Y Karnik and Mrdjan Jankovic. Imc based wastegate control using a first order model for turbocharged gasoline engine. *2012 American Control Conference*, pages 2872 – 2877, 2012. doi: http://dx.doi.org/10.1109/ACC.2012.6315144. Cited on pages 4, 17, 18, and 39.

Oskar Leufven. *Modeling for control of centrifugal compressors*. PhD thesis, Linköping University, 2013. Cited on pages 4, 7, and 15.

Lennart Ljung and Torkel Glad. *Modellbygge och Simulering, andra upplagan*. Studentlitteratur, Lund, 2004. Cited on page 53.

Farouq Meddahi, Alain Charlet, Yann Chamaillard, and Christian Fleck. Incorporating thermo- and aerodynamic losses into compressor models for real-time applications. In *SAE Technical Paper*. SAE International, 04 2015. doi: 10.4271/2015-01-1715. URL http://dx.doi.org/10.4271/2015-01-1715. Cited on page 4.

Martin Müller, Elbert Hendricks, and Spencer C. Sorenson. Mean value modelling of turbocharged spark ignition engines. In *SAE Technical Paper*. SAE International, 02 1998. doi: 10.4271/980784. URL http://dx.doi.org/10.4271/980784. Cited on page 4.

Paul Moraal and Ilya Kolmanovsky. Turbocharger modeling for automotive control applications. In *SAE Technical Paper*. SAE International, 03 1999. doi: 10.4271/1999-01-0908. URL http://dx.doi.org/10.4271/1999-01-0908. Cited on page 4.

Davide Moro, Enrico Corti, Matteo De Cesare, and Gabriele Serra. Upgrade of a turbocharger speed measurement algorithm based on acoustic emission. In *SAE Technical Paper*. SAE International, 04 2009. doi: 10.4271/2009-01-1022. URL http://dx.doi.org/10.4271/2009-01-1022. Cited on page 3.

Chunsheng Ni, Gangand Xi, and Hui Guo. 涡轮增压器电动废气门精确开度控制的研究. *Shanghai Auto*, 8:28–32, 08 2013. Cited on pages 3, 4, and 51.

Mattias Nyberg and Erik Frisk. *Model Based Diagnosis of Technical Processes, Course Material in Diagnosis and Supervision.* Bokakademin Linköping, 2014. Cited on page 51.

Fabrizio Ponti, Vittorio Ravaglioli, Enrico Corti, Davide Moro, and Matteo De Cesare. Non-intrusive methodology for estimation of speed fluctuations in automotive turbochargers under unsteady flow conditions. *SAE Int. J. Engines*, 7:1414–1421, 04 2014. doi: 10.4271/2014-01-1645. URL http://dx.doi.org/10.4271/2014-01-1645. Cited on page 3.

Andreas Thomasson, Lars Eriksson, Oskar Leufven, and Per Andersson. Wastegate actuator modeling and model-based boost pressure control. In *IFAC Workshop on Engine and Powertrain Control, Simulation and Modeling*, Paris, France, 2009. Cited on pages 4 and 97.

Andreas Thomasson, Oskar Leufvén, Ivan Criscuolo, and Lars Eriksson. Modeling and validation of a boost pressure actuation system for a series sequentially turbocharged SI engine. *Control Engineering Practice*, 21:1860–1870, 2013. Cited on pages 11 and 97.

Kazuhide Togai and Naoto Fujinaga. A reduced order model for a passenger car turbo charging system and application to engine output torque profile control. In *SAE Technical Paper*. SAE International, 09 2015. doi: 10.4271/2015-01-1981. URL http://dx.doi.org/10.4271/2015-01-1981. Cited on page 5.

G. Winkler. *Steady-State and Dynamic Modelling of Engine-Turbomachinery Systems.* PhD thesis, University of Bath, 1977. Cited on page 14.